CHALMERS

Simulation of Gravitational Waves and Binary Black Holes Space-times

Master's Thesis in Masters Degree Programme, Radio and Space Science

FAHAD NASIR

Department of Fundamental Physics
CHALMERS UNIVERSITY OF TECHNOLOGY
Göteborg, Sweden 2010.

Simulation of Gravitational Waves and Binary Black Holes Space-times
Overview of Gravitational Wave Science. Extraction of Gravitational Waves with post-Newtonian Approximation and Numerical Relativity Formulation

FAHAD NASIR,

Examiner: Martin Cederwall

Department of Fundamental Physics
Chalmers University of Technology
SE-412 96 Göteborg
Sweden
Telephone + 46 (0)31-772 1000

Department of Fundamental Physics
Göteborg, Sweden January 2010

Simulation of Gravitational Waves and Binary Black Holes Space-times

Fahad Nasir

Department of Fundamental Physics
Chalmers University of Technology

Abstract

The main objective of this thesis is to study gravitational radiation along with its associated phenomena, specifically for binary black holes. The occurrence of such events in our universe have profound implications when gravitational waves are radiated by accelerating massive astrophysical bodies. The specific system under our consideration is a binary black hole. The two essential phases of binary black hole, namely inspiral and merger have their characteristic gravitational wave signature. Gravitational waves during these phases are obtained by taking advantage of powerful numerical tools available. Two popular techniques are applied to determine waveforms, namely post-Newtonian approximation for the inspiral phase and numerical relativity techniques for the merger phase of binaries.

The nature of gravitational wave is explained by considering the linearised theory of general relativity and its effect on free-falling bodies. A detailed description of the multipole expansion is provided which also encompasses the famous Einstein quadrupole formula. For the inspiral phase of binary black holes, the post-Newtonian formalism is discussed in detail. Extraction of waveforms by the post-Newtonian method is implemented by MATLAB routines to test the findings. Lastly, the foundation of numerical relativity is reviewed which serves the purpose to carry out further discussions on gravitational waves in strong gravity regime during merger phase of binaries. ADM and BSSN formalism is introduced along with the Schwarzschild and Misner initial data. BSSN evolution of Misner initial data is carried out by CCATIE code. The Weyl scalars are extracted to provide an invariant way of representing outgoing gravity waves at various stages of evolution.

Acknowledgements

I express my gratitude to my supervisor, Martin Cederwall for his kind help and support. Without his exhilaration and encouragement this work would not have been possible. The discussions proved to be really conducive and kept me motivated throughout the whole thesis work. I am grateful to the department of Fundamental Physics for providing me the opportunity. I am thankful to the department of Radio and Space for providing the necessary theoretical foundation which made all this effort conceivable. Special thanks to John H. Black for introducing me to our strange universe of black holes and quasars . Finally, I be indebted to my room-mates, Hassan and Junaid, for such refreshing discussions during stress times.

Contents

1 Introduction

General relativity was formulated by Einstein on the foundation of the equivalence principle. Gravity waves travelling at speed of light is an inevitable consequence of such a principle. A gravitational wave (GW) can be regarded as a fluctuation in space-time which travel outwards carrying energy from source. Such ripples in space-time are the result of complex dynamics of massive dense objects or due to the interaction of massive stars, black holes or neutron stars binaries. Once produced, they can travel unhindered straight to the earth without much interaction with the matter. Such disturbance appear as distorted space-time to a distant observer. However our earth is minuscule compare to the wavelength of GW, as distances are so tremendous that their detection is huge challenge posed by modern astronomy.

After Einstein had formulated his theory of general relativity, within months he figured out the famous quadrupole formula for gravitational waves, which is valid for bodies with negligible self-gravity. Till mid 1920s, linearised theory was understood due to the contributions by Weyl (1922) and Eddington (1924). Landau and Lifshitz gave the first theoretical treatment of radiation emission by self-gravitating bodies [2]. However in 1940's and 1950's, scientific community was not considering GW as a physical possibility to carry energy from the system. Feynman proposed “Sticky Bead” thought experiment to prove the existence of such waves carries energy. The thought experiment states that any passing wave should move any bead on stick back and froth, hence producing friction and thus concluding that wave carries energy. Later on Bondi, Weber and Wheeler developed the formalism based on Feynman argument. Bar detectors were build around the world to detect waves from various astrophysical sources. The effort was initiated by Weber which eventually detected electrical signals at two bar detectors (one at chicago and other near Washington DC) simultaneously. In 1970s, soviet scientist suggested to develop Michelson-Morley interferometers for detection of gravitational waves. In 1973, a major breakthrough happened, when Taylor and Russell Hulse detected pulsar 1913+16 which was in a binary. The orbital decay (76.5 ms per year) was precisely consistent with the energy carried away by the waves as predicted by general relativity. In 2003, another major binary pulsar J0737-3039 was discovered, which also agrees well with predictions of general relativity. The technological efforts made in 70's contributed to the second generation of detectors with advanced cooling techniques. Several interferometers are now operating around the world like LIGO, GEO, VIRGO and TAMA. The bursts sensitivity now has reached Khz ($h \sim 10^{-17}$) increasing the possibility of detecting such an event to about 3/yr. The sensitivity of detectors can be divided into high ($f \geq 10\,Hz$), low ($10^{-5}\,Hz \leq f \leq 10\,Hz$) and extremely low ($f \leq 10^{-5}\,Hz$) frequency bands. For detailed discussion on history of gravitational wave research, see [2,22,25].

Gravitational waves provide a possible way to probe the distant universe and test exotic theories related to cosmology, the early universe and extreme gravitational regimes. The differences mentioned in table 1.1. mark gravitational waves astronomy as revolutionary and will potentially have much more profound impact as compared to radio waves astronomy. However we know that the electromagnetic astronomy is mature and well established field so the promises seem blown out of proportion. The possible reason for this is that source distances or strengths are uncertain with several orders of magnitude, with the exception of binaries.

In the future, possible detection of GW may give us extensive information about the universe and make it possible to test physical laws which can never be tested by any other method known to date. When gravitational waves and light arrive to earth from a astrophysical source it should confirm the prediction of general relativity that the light and gravity waves both travels with same speed. The polarisation of gravitational waves may confirm that the gravitons are transverse traceless and gravitons have spin 2.

The primary purpose of simulating the binaries and supernovae bursts is to extract waveforms and compare them with the ones obtained from the actual sources which can eventually confirm the dynamics of the system predicted by general relativity. This will not only prove the existence of black holes but provide ample clue for determining various physical features of the system. Moreover, GW astronomy can offer a very strict test to general relativity in strong gravitational field.

The greatest challenge with such simulations is to extract waveforms to an accuracy which can be matched filtered with the noisy waveform received. Matched filtering with a bank of waveforms results in identifying and estimating the various parameters in the dynamics of the source. Post-Newtonian approximations are popular to produce waveform banks when proper numerical tools are incorporated [24].

An even great challenge is to simulate the extreme space-time around binaries when post-Newtonian approximations are not anymore accurate. In such situations Baumgarte-Shapiro-Shibata-Nakamura (BSSN) formalism of Einstein's equations proved to provide stable simulations with constrained evolutions [1,15,16,17].

Table 1.1. The comparison between for electromagnetic and gravitational waves

Electromagnetic Waves	Gravitational Waves
Accelerating charges produce time changing dipole moments	Accelerating masses produce time changing quadrupole moments
Incoherent superposition of radiation from electrons, atoms, and molecules	Coherent superposition of radiation from the huge dense mass source like black hole and massive stars
Information about the thermodynamics of the system	Direct information about the dynamics of the system
Wavelength small compared to the source	Wavelength are large compared to the source
Scattered, absorbed by the matter	Negligible interaction with the matter
Very high frequency ranges (observation frequencies at KHz and MHz)	Very low frequency range (frequencies range is several orders less then 10Hz)

Outline

In chapter 2, a very quick review of gravitational wave sources is given. We have tried to possibly list all the primary GW sources with their brief description. Description of how GW are studied in various bandwidth, provide profound information about universe.

Chapter 3 is the very foundation of gravitational radiation. Basic concepts are discussed and formalism is introduced. The very nature of GW is explored by linearised general relativity. The multipole decomposition of field is the key concept developed in this chapter.

In chapter 4, we starts with a description of post-Newtonian approximation with all its limitations and applications. The post-Newtonian expressions are being implemented by MATLAB routines and results are discussed.

The last chapter is a precise description of topics concerning numerical relativity. The essential formulations are introduced which are crucial for binary evolution problem. Schwarzschild and Misner initial data are discussed and the results for their evolution are presented.

2 Gravitational Wave Sources

Theoretically, any mass that accelerates is a source of gravitational waves. From an accelerating meteoroid in an orbit around sun to inspiralling black holes or even exploding supernovae, all are sources of radiation. Unfortunately the strengths of such sources are much weaker, or when the wave reaches earth its become painfully feeble, making extremely challenging to detect. The sources vary from binaries to the supernovae bursts where each phenomenon has its own characteristic GW, giving clues about the dynamics of the system. The most common type of dynamics we deal with is of binaries. To describe a simple binary system, one assumes two huge astrophysical objects which orbit around some centre of mass which depends on magnitude of two masses (in the centre, for equal size binary). Such masses can be neutron stars or even black holes. However, stars like our sun generate radiation at such a small scale that its detectability is impossible with our present technology or even in near future. When binaries inspiral they move deep into a potential well giving its excess energy in form of radiation. The orbit become smaller and smaller, eventually this downward inspiral results in coalescence of the two bodies. When the binary become effectively one body its rotation of non-spherical shape also results in GW. Now, we will briefly discuss some of the wave sources with all their associated phenomena.

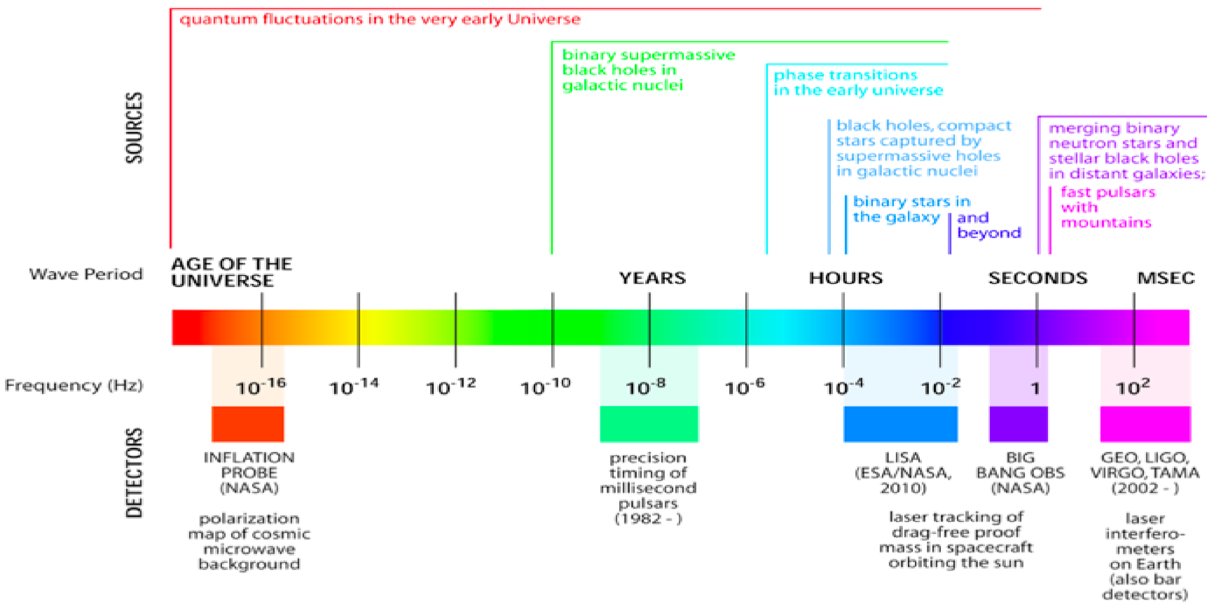

Figure 2.1. Various frequency bands in GW astronomy are shown along with the mechanism causing the radiation. Universe phase transitions, cosmic strings and domain walls are some of the exciting futuristic subjects which can be studied by radiation. GW emission from binary black holes and neutron stars are studied at low frequencies and high frequencies bands which is of principle interest in our work.

2.1 Binary Black Hole Mergers

Stellar mass black holes exist in galaxies and globular clusters (stars clusters orbiting in galactic core). Supermassive black holes can form at galactic nuclei due to the merger of galaxies. The inspiral and merger of black hole is strange and extremely interesting to observe. Such mergers are one of the spectacular sources of radiation. The black holes are extremely dense objects, thus results in much less coalescence time and a lot of fascinating radiation. Stellar mass black holes emit GW in the high frequency band and have been probed by Laser Interferometer Gravitational Observatory (LIGO), while waves in the low frequency band will be studied by Laser Interferometer Space Antenna (LISA) [27]. The information provided by binary black hole waveforms is profound. The surface areas, masses, spins, orbits in curved space-time and nonlinear dynamics, can all be established from the waveform signature. Moreover, we can test the Penrose cosmic censorship conjecture, the second law of black hole mechanics and how they pulsate and lose their excess hair by radiation. Gravitational waveforms can be extracted by various methods in different phases of the binaries. Inspiral phase waveforms can be extracted by post-Newtonian approximation, merger by numerical relativity and finally ring-down by perturbation theory.

Table 2.1. Showing the equipment designed for GW observation, the distance they are able to probed along with their respective signal to noise ratios (SNR) for binaries [27].

Equipment	Distance	Event Rate	SNR
LIGO and Initial Interferometers	100 Mpc	1/200 yr to 1/yr	10 or less
LIGO and Advanced Interferometers	$z\sim0.4$	2/month to 15/day	10 to 100
LISA	$z\sim10$	few/yr	100 to 100,000

2.2 Neutron Star or Small Black Hole Inspiral into Supermassive Black Hole

Supermassive black holes are mostly located at the galactic nuclei. Occasionally small black holes and neutron stars inspiral and finally plunge into such supermassive black holes resulting in a myriad of radiation. The rate of such events are about few per year to the distances probe by LISA. Such GW waveform probe into galactic nuclei and supermassive black hole space-time. Waves are emitted in the low frequency spectrum. Mapping black hole, evolution of horizons and test of no hair theorem are one of the exotic conjectures which can be tested with such data. Black hole perturbation theory is the key framework for obtaining such waveforms.

2.3 Neutron Star and Black Hole Mergers

The existence of such events can be found in globular clusters. Initially the neutron star and the black hole go into a downward inspiral, and eventually the neutron star forms lobes which are sucked into black hole. GW emitted usually lies in the high frequency band. Initial interferometers have probed to 43 Mpc with event rate $1/2500\,\mathrm{yr}-1/2\,\mathrm{yr}$. Advanced interferometers rates can quest up to at 650 Mpc with occurrence rate $1/\mathrm{yr}-4/\mathrm{day}$.

Waves convey information about the spin, orbit, masses, tidal disruption of neutron star and its structure. Theories about neutron star evolution and its equation of state for matter can be tested and verified. Both post-Newtonian and numerical relativity techniques are employed to obtain waveforms depending on the phase of binaries.

2.4 Neutron Star and Neutron Star Inspiral

Such events can happen when main sequence progenitors in the galaxy capture binaries in globular clusters. Waves are emanated in the high frequency band. Initial interferometers have studied distances up to 200 Mpc with rates 1/3 yr^{-1} - 1/300 yr^{-1} while advanced interferometers up to 300Mpc with rates 1/yr - 3/day. Information carried by waveform is about masses, spins, and orbit during inspiral phase. But during merger phase information is lost due to high noise of equipment. Relativistic effects can be studied during inspiral phase. The method for extraction of waveforms is post-Newtonian approximation.

2.5 Spinning Neutron Stars or Pulsars

Spinning neutron stars are known as pulsars and lie the in high frequency band of the spectrum. Pulsar rotation rates are found to be ~ 250-700 rev/s. The mountains on the surface of neutron stars cause emission of radiation, which tries to reduce the spin of star. However, spin rates are kept in this limit when radiation torque is in balance with the accretion disc torque around neutron star. In such steady state, X-ray luminosity (due to rate of accretion of mass around neutron star) is proportional to wave strength. Detectability of the star depends on the spin and ellipticity of the pulsating neutron star. Pulsar ellipticity is generally of order $\epsilon \leq 10^{-6}$. Ellipticity also decides the frequency of pulsars. GW helps probing neutron star structure and its behaviour during birth. Slow motion and strong gravity techniques are used for analysis of the problem. Both X-ray luminosity and GW yield information about the temperature, crust and viscosity of the neutron star.

2.6 Neutron Star Birth

Neutron stars can be formed due to supernovae explosions or due to the collapse of accretion induce white dwarf. R-mode (radial modes of vibration) instability depends on the spin of the neutron star. If period of spin is less then 10^{-3} s, then neutron star is R-mode unstable. Moreover the GW emission drives the R-mode sloshing. We still don't have evidence what stops the growth of sloshing at later stages. GW give us insight about crust formation, coupling of R-modes, wave breaking, shock formation and magnetic field torques. Any of these can be the reason of stopping sloshing growth.

Figure 2.2. R sloshing of spinning neutron star causes emission of GW

2.7 Gravitational Waves from Early Universe

Gravitational waves were originated even during the big bang, but the expansion of universe red-shifted the waves. Inflation results in amplification of quantum fluctuations which leads to primordial GW. As time progresses the fundamental forces of universe decoupled, causing phase transitions, which again produce GW. Electroweak phase transition (~100 GeV) occurred when universe was about 10^{-11} s old. LISA can probe to electroweak phase transition, while LIGO can probe to phase transition which has occurred at ~10^{9} GeV or when age of universe was ~10^{-25} s old. Waves in all bands provide information about early universe phases. Inflation can be studied by cosmic microwave background anisotropy at extremely low frequencies. GW can inquest into physics of big bang, inflation and equation of state of very the primitive universe. Quantum gravity and cosmological perturbation theory can assist the study and analysis of waveforms. Such studies can help to determine strength of electroweak phase transition, and to probe evolution of inhomogeneities produced by phase transition.

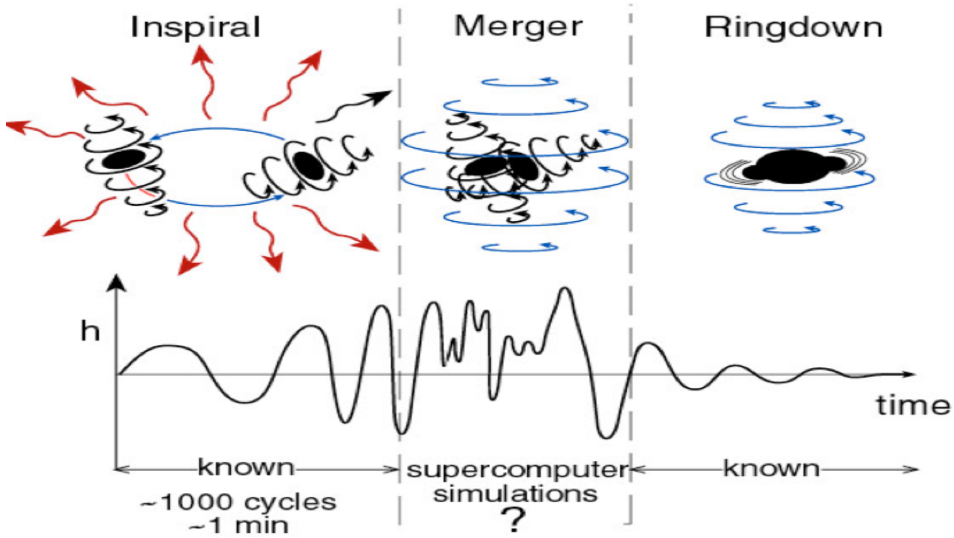

Figure 2.3. Three phases of gravitational radiation from binary black hole source. The inspiral phase involves the post-Newtonian expansion while the merger requires numerical relativity techniques to extract the waves. The ring-down phase can essentially be treated as effective single body with small perturbations.

3 Gravitational Radiation

Gravitational radiation is fundamentally ripples in space-time, which travels with speed of light and cause distance between free falling objects to vary. The distance between floating objects is stretched and squeezed by a passing wave. It can be lensed, red-shifted and scattered (significantly by massive dense objects like black holes) like the electromagnetic waves. However absorption and dispersion of GW by matter is negligible which is the reason wave can travel without hindrance through galactic nuclei and massive stars. The essential non-linearity adds complexity to the problem.

The basic assumption before treating any cosmological problem, that universe is isotropic and homogenous on large scale is our guiding principle. This endorses that the average curvature of universe is intrinsically the same. We have clues about curvature of universe globally. We may reason that the universe may have zero (flat), positive or negative curvature. However the problem of determining the curvature locally is extremely difficult due to non-linearity of gravity. The information provided by the Riemann curvature tensor in this regard is extensive as suggested by general relativity. We can define such a tensor conveying information about curvature of universe globally. A gravitational wave also contributes to the curvature of the universe. However, scales of contribution for both curvatures may vary largely. To mathematically elaborate the concept of gravitational waves we need to consider how the curvature of the universe can be conceived and how it adds to the Riemann tensor which is treated by short wave approximation [2,7].

3.1 Short Wave Approximation

A major problem concerning gravity is its non-linearity. It is not possible to precisely separate the contribution of GW from the curvature of space-time. The length scales on which it varies (λ_{GW}) is much shorter compare to all other important curvatures in astrophysical situations. This significant difference make possible to split the Riemann tensor into two, one is background ($R^{B}_{\mu\nu\sigma\rho}$) part and other is GW part ($R^{GW}_{\mu\nu\sigma\rho}$). The split is not analytically accurate but it's a very worthy approximation. The $R^{B}_{\mu\nu\sigma\rho}$ can be regarded as the global large scale average curvature of universe over several wavelengths. $R^{GW}_{\mu\nu\sigma\rho}$ is the rapidly changing part of the Riemann tensor describing small scale curvature locally. The following expressions estimate their respective scales

$$R^{B}_{\mu\nu\sigma\rho} \sim \frac{1}{R^2} \tag{3.1.1}$$

$$R^{GW}_{\mu\nu\sigma\rho} \equiv R_{\mu\nu\sigma\rho} - R^{B}_{\mu\nu\sigma\rho} \sim \frac{h}{\lambda^2_{GW}} \tag{3.1.2}$$

where R is the Ricci scalar and λ_{GW} is the wavelength of GW divided by 2π. We have considered $R^{B}_{\mu\nu\sigma\rho}$ inversely proportional to R^2 assuming a closed universe, like the curvature of closed sphere is defined as inverse square of its radius. We can have an approximation of how the magnitude of two parts of Riemann tensor differ, following calculation for the GW wavelength probed by LIGO ($h \sim 10^{-22}$) can be done.

$$\frac{1}{R^2} \sim \frac{1}{10^{56}\,\mathrm{cm}^2} \tag{3.1.3}$$

$$R^{GW}_{\mu\nu\sigma\rho} \sim \frac{h}{\lambda^2_{GW}} \sim \frac{10^{-22}}{(10^8\,\mathrm{cm})^2} \sim \frac{1}{10^{-38}\,\mathrm{cm}^2} \gg \frac{1}{10^{56}\,\mathrm{cm}^2} \tag{3.1.4}$$

where R is approximated by Hubble radius of universe. This powerful method of defining GW part of Riemann tensor was introduced by Wheeler and Power (1957) and is known as two length expansion or short wave approximation. The pertinent result is that GW truly behaves in the same way as electromagnetic waves in vacuum.

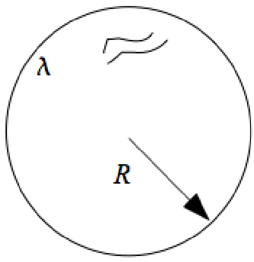

Figure 3.1. Shows a closed universe scenario where metaphorically the closed world is like an orange and its surface ripples are like scale of GW wavelength.

3.2 Equation of Geodesic Deviation

To illustrate how the incoming wave influences the free-falling particles we need to consider how the geodesics of two particles deviate. We will derive the fundamental equation for geodesic deviation in terms of the Riemann tensor. We can assume two free-falling point particles A and B as shown in the Figure 3.2. with their respective trajectories $x^\mu(\tau)$and $x^\mu(\tau)+\xi^\mu$. By geodesic equation for a particle we have their corresponding equations.

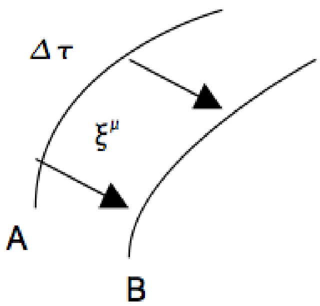

Figure 3.2. Two particles A and B moving through space-time

$$\frac{d^2x^\mu}{d\tau^2} + \Gamma^\mu_{\nu\lambda}\frac{dx^\nu}{d\tau}\frac{dx^\lambda}{d\tau} \tag{3.2.1}$$

$$\frac{d^2(x^\mu+\xi^\mu)}{d\tau^2}+\Gamma^\mu_{\nu\lambda}(x+\xi)\frac{d(x^\nu+\xi^\nu)}{d\tau}\frac{d(x^\lambda+\xi^\lambda)}{d\tau} \tag{3.2.2}$$

Taking the difference of these two equations mentioned above and ignoring second and higher order terms in ξ^μ we can simply derived the equation for geodesic deviation.

$$D_u D_u \xi^\mu = R^\mu_{\nu\sigma\rho}\xi^\sigma U^\nu U^\rho \tag{3.2.3}$$

where $U^\sigma = d\xi^\sigma/d\tau$ is the velocity of particle and D_u is the associated covariant derivative.

3.3 Mathematical Description of Gravitational Wave

Lets consider two test particles A and B in nearly flat Minkowski space-time. Particle A is in rest in the local Lorentz frame of our observer. As the gravitational waves passes, the particle B appears to be moving as seen by observer shown in the Figure 3.3.

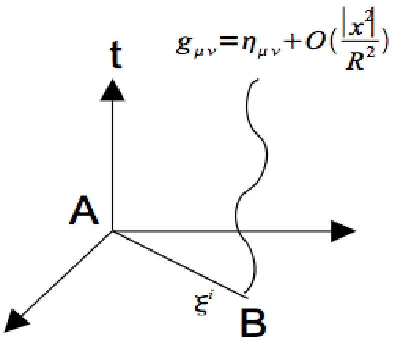

Figure 3.3. In local Lorentz frame of A, particle B seems to moving when GW is passing where metric tensor $g_{\mu\nu}$ is approximated by the considering closed Friedmann Walker universe scenario and assuming $|R_{\mu\nu\rho\sigma}| \sim 1/R^2$.

Let ξ^i be the general coordinate distance, then the variation in distance when GW are passing by is

$$\xi^i = \xi^i_{(0)} + \delta\xi^i \tag{3.3.1}$$

where $\xi^i_{(0)}$ is the initial distance before the wave. By the condition of geodesic deviation (3.2.3) we have

$$\frac{\partial^2}{\partial t^2}\xi^i = -R^i{}_{0j0}\,\xi^j \tag{3.3.2}$$

As there was no relative motion between particles A and B before, (3.3.2) by aid of (3.3.1) reduces to

$$\frac{\partial^2}{\partial t^2}\delta\xi^i = -R^i{}_{0j0}\xi^j \tag{3.3.3}$$

Remember that in local Lorentz frame all the components of the Riemann tensor are determined by R_{i0j0}. By defining the field metric

$$-R^i{}_{0j0} = \frac{1}{2}\ddot{h}_{ij}^{TT} \tag{3.3.4}$$

we can simplify the expression

$$\frac{\partial^2}{\partial t^2}\delta\xi^i = \frac{1}{2}(\ddot{h}_{ij}^{TT}\xi^j(0)) \tag{3.3.5}$$

or

$$\delta\xi^i = \frac{1}{2}(h_{ij}^{TT}\xi^j(0)) \tag{3.3.6}$$

Now to visualize how the passing GW effect free floating particles, we will consider the following scenario. When the wave is propagating only in the z-direction, the effect on x-y plane circle can be explained by (3.3.6). We have a set of four equations for our current circle. The expressions can be categorized as two modes of vibration (plus and cross modes) depending on the value of field. Figure 3.4 illustrates the effect of this passing wave. For the plus mode of vibration the equations are

$$\delta x = \frac{1}{2}(h_{plus}^{TT}x(0)) \tag{3.3.7}$$

$$\delta y = -\frac{1}{2}(h_{plus}^{TT}y(0)) \tag{3.3.8}$$

Similarly, for the cross mode we have

$$\delta x = \frac{1}{2}(h_{cross}^{TT}y(0)) \tag{3.3.9}$$

$$\delta y = \frac{1}{2}(h_{cross}^{TT}x(0)) \tag{3.3.10}$$

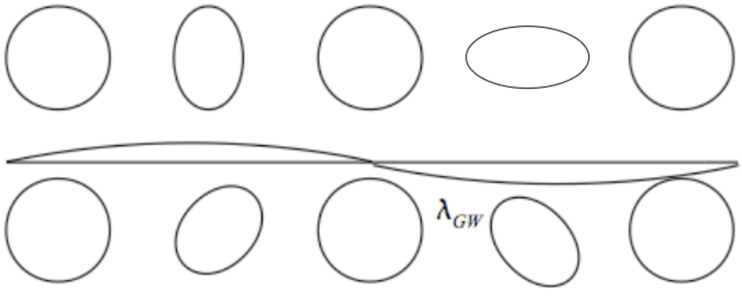

Figure 3.4. Considering points on a circle in x-y plane. As GW passes in z-direction how distance between points varies is shown for the both modes of vibration. It is apparent that field reinstate its initial configuration after cycle of wave.

3.4 Linearised Einstein's Equations

Einstein's equations by equivalence principle are given by

$$G_{\mu\nu} \equiv R_{\mu\nu} - \frac{1}{2} R = 8\pi T_{\mu\nu} \tag{3.4.1}$$

where $T_{\mu\nu}$ is the energy momentum tensor, R the Ricci scalar and $R_{\mu\nu}$ the Ricci tensor. The Einstein's equations can be thought as 10 coupled second order partial differential equations for ten metric tensor components. Again the non-linearity makes it demanding to find an exact solution of Einstein's equations. The best way to understand wave nature of GW is by finding a solution of Einstein's equations (3.4.1) in a linearised regime [28]. We will assume a region far away from any source which is nearly flat regime. The metric can then be expressed as sum of Minkowski flat metric plus small perturbations.

$$g_{\mu\nu} = \eta_{\mu\nu} + h_{\mu\nu} \tag{3.4.2}$$

where $\eta_{\mu\nu}$ is Minkowski space-time with metric signature $\eta_{\mu\nu} = (-1,1,1,1)$ and perturbations are small $|h_{\mu\nu}| \ll 1$. Partial derivatives of the metric can readily calculated as

$$g_{\mu\nu,\alpha} = \eta_{\mu\nu,\alpha} + h_{\mu\nu,\alpha} = h_{\mu\nu,\alpha} \tag{3.4.3}$$

We know the general expression of Christoffel symbols in terms of metric tensor

$$\Gamma^{\mu}_{\alpha\beta} = \frac{1}{2} g^{\mu\nu} (g_{\nu\alpha,\beta} + g_{\beta\nu,\alpha} - g_{\alpha\beta,\nu}) \tag{3.4.4}$$

We can linearised expression this expression with the aid of equations (3.4.3) and (3.4.2)

$$\Gamma^{\mu}_{\alpha\beta} = \frac{1}{2} \eta^{\mu\nu} (h_{\nu\alpha,\beta} + h_{\beta\nu,\alpha} - h_{\alpha\beta,\nu})$$

$$= \frac{1}{2} (h^{\mu}_{\alpha,\beta} + h^{\mu}_{\beta,\alpha} - h_{\alpha\beta,}{}^{\mu}) \tag{3.4.5}$$

Another expression we need is of the Riemann curvature tensor in terms of Christoffel symbols

$$R_{\mu\nu} = \Gamma^{\rho}_{\mu\nu,\rho} - \Gamma^{\rho}_{\mu\rho,\nu} + \Gamma^{\rho}_{\rho\sigma}\Gamma^{\sigma}_{\nu\mu} - \Gamma^{\rho}_{\nu\sigma}\Gamma^{\sigma}_{\rho\mu} \tag{3.4.6}$$

by use of the (3.4.5) and by neglecting the second and higher order term which is valid for the linearised regime, (3.4.6) reduces to

$$R_{\mu\nu} = \Gamma^{\rho}_{\mu\nu,\rho} - \Gamma^{\rho}_{\mu\rho,\nu}$$

$$= \frac{1}{2}\left(h_{\mu\ ,\nu\rho}^{\ \rho} + h_{\nu\ ,\mu\rho}^{\ \rho} - h_{\mu,\nu\rho}^{\ \ \ \ \rho} + h_{,\mu\nu}\right) \tag{3.4.7}$$

Moreover, the Ricci scalar can be approximated as

$$R \equiv g^{\mu\nu} R_{\mu\nu} \approx \eta^{\mu\nu} R_{\mu\nu} \tag{3.4.8}$$

By use of (3.4.8), (3.4.7) and substituting it in (3.4.1) we have

$$\left(h_{\mu\ ,\nu\rho}^{\ \rho} + h_{\nu\ ,\mu\rho}^{\ \rho} - h_{\mu,\nu\rho}^{\ \ \ \ \rho} + h_{,\mu\nu}\right) - \eta_{\mu\nu}\left(h_{\sigma\rho}^{\ \ \ \sigma\rho} - h_{,\sigma}^{\ \ \sigma}\right) = 16\pi T_{\mu\nu} \tag{3.4.9}$$

For the purpose of simplification, we will define new trace inverse metric tensor

$$\bar{h} \equiv h_{\mu\nu} - \frac{1}{2}\eta_{\mu\nu} h \tag{3.4.10}$$

solving again (3.4.9) for this new metric, we acquire our equation

$$\bar{h}_{\mu\nu\rho}^{\ \ \ \ \ \rho} + \eta_{\mu\nu}\bar{h}_{\rho\sigma}^{\ \ \ \rho\sigma} - \bar{h}_{\mu\rho,\nu}^{\ \ \ \ \ \rho} - \bar{h}_{\nu\rho,\mu}^{\ \ \ \ \ \rho} = 16\pi T_{\mu\nu} \tag{3.4.11}$$

Now using the Lorenz gauge condition $\bar{h}_{\mu\rho,}^{\ \ \ \ \rho} = 0$ we have finally our desired result.

$$\bar{h}_{\mu\nu\rho}^{\ \ \ \ \ \rho} = -16\pi T_{\mu\nu} \tag{3.4.12}$$

which has the familiar Green's function as a solution

$$\bar{h}_{\mu\nu} = -4\frac{\int T_{\mu\nu}(\vec{x}', t - |\vec{x} - \vec{x}'|)}{|\vec{x} - \vec{x}'|} dV' \tag{3.4.13}$$

The simplest solution one can have for (3.4.13) is plane wave solution of the form

$$\bar{h}_{\mu\nu} = \Re\left(A_{\mu\nu} e^{ik_a x^a}\right) \tag{3.4.14}$$

where $A_{\mu\nu}$ is the polarization tensor and $k^{\mu} = (\omega, \vec{k})$, with the gauge conditions

$$k_{\mu} k^{\mu} = 0 \tag{3.4.15}$$

$$k_{\nu} A^{\mu\nu} = 0 \tag{3.4.16}$$

Using the Lorenz gauge condition we can determine the only radiative components of the field metric ($h_{\mu\nu}^{TT}$), so we reduce to transverse traceless gauge. If we assume the wave travels in the z -direction and by imposing the gauge conditions (3.4.15) and (3.4.16) we have

$$A_{0z} = A_{xz} = A_{yz} = A_{zz} = 0 \tag{3.4.17}$$

for the linear regime equation (3.4.16) can be rewritten as

$$A_{\mu\nu}\eta^{\mu\nu} = 0 \tag{3.4.18}$$

which implies the condition

$$A_{xx} = -A_{yy} \tag{3.4.19}$$

By conditions (3.4.17) and (3.4.19) we finally have our polarization tensor.

$$A_{\mu\nu} = \begin{pmatrix} 0 & 0 & 0 & 0 \\ 0 & A_{xx} & A_{xy} & 0 \\ 0 & A_{xy} & -A_{xx} & 0 \\ 0 & 0 & 0 & 0 \end{pmatrix} \tag{3.4.20}$$

The polarization tensor (3.4.20) indicates that we reduce to just two degrees of freedom in transverse traceless gauge which are intrinsically two (plus and cross) modes of GW.

$$A_{plus} = \begin{pmatrix} 0 & 0 & 0 & 0 \\ 0 & 1 & 0 & 0 \\ 0 & 0 & -1 & 0 \\ 0 & 0 & 0 & 0 \end{pmatrix} \tag{3.4.21}$$

$$A_{cross} = \begin{pmatrix} 0 & 0 & 0 & 0 \\ 0 & 0 & 1 & 0 \\ 0 & 1 & 0 & 0 \\ 0 & 0 & 0 & 0 \end{pmatrix} \tag{3.4.22}$$

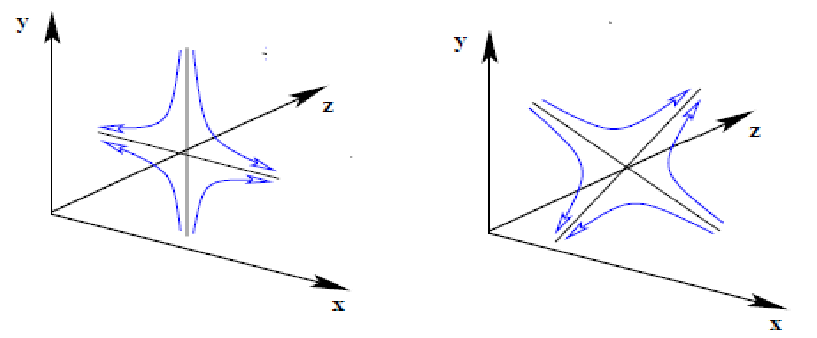

Figure 3.5. F … sented like the electromagneti …

Table 3.1. … itional field by rotation of ang … ves is 1 and for GW is 2. Tra … where h is the helicity of the

Electromagnetic waves	Gravitational waves
$E_x^{new} = E_x \cos\theta + E_y \sin\theta$ $E_y^{new} = E_y \cos\theta - E_x \sin\theta$	$h_{plus}^{new} = h_{plus} \cos 2\theta - h_{cross} \sin 2\theta$ $h_{cross}^{new} = h_{cross} \cos 2\theta + h_{plus} \sin 2\theta$

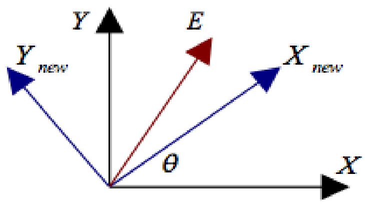

Figure 3.6. Rotation of an electric field by an angle θ

3.5 Multipole Moments Decomposition

Multipole expansions are useful express to any field potential around any source in series expansion which often can be truncated to some term. The same is true for the gravitational field of mass source as well as for electromagnetic field around a point charge. For detailed discussion on this topic, see [5,12]. First we will describe how the multipole expansion of Maxwell's equations can be done which eventually guides us how to expand a classical gravitational field. Maxwell's equations can be written in covariant form as

$$\partial_\nu F^{\mu\nu} = J^\mu \tag{3.5.1}$$

$$F_{\mu\nu} = \partial_\mu A_\nu - \partial_\nu A_\mu \tag{3.5.2}$$

where $A_\mu = (\phi/c^2, -\vec{A})$ and $J^\mu = (\rho, \vec{J})$, by substituting (3.5.2) in (3.5.1)

$$\partial_\nu \partial^\mu A^\nu - \partial_\nu \partial^\nu A^\mu = J^\mu \tag{3.5.3}$$

Again exploiting the gauge freedom we have, Lorenz gauge simplifies the expression (3.5.3)

$$\partial_\nu \partial^\nu A^\mu = -J^\mu \tag{3.5.4}$$

(3.5.4) has the famous Green's function as a general solution

$$A^\mu(\vec{x}, t) = \frac{-\int J^\mu(\vec{x}', t - |\vec{x} - \vec{x}'|/c)}{|\vec{x} - \vec{x}'|} dV' \tag{3.5.5}$$

Now considering a region far away from the source such that $|x| \gg R$, where R is the size of the source. The power series expansion of factor $|\vec{x} - \vec{x}'|^{-1}$

$$\frac{1}{|\vec{x} - \vec{x}'|} = \frac{1}{\sqrt{(\vec{x} - \vec{x}')^2}} = \frac{1}{\sqrt{\vec{x}^2 - 2\vec{x}\,\vec{x}' + \vec{x}'^2}} = \frac{1}{|\vec{x}|} + 2\,\vec{x}'.\vec{n}\frac{1}{|\vec{x}|^2} + \ldots \tag{3.5.6}$$

where $\vec{n}=\vec{x}/|\vec{x}|$. Now consider the retarded time factor as nearly constant we can expand the difference as

$$t-t_0=(|\vec{x}|-|\vec{x}-\vec{x}'|)/c=-\vec{n}.\vec{x}'/c+O(|x|^{-1}) \tag{3.5.7}$$

hence by (3.5.7) the J^{μ} term in (3.5.5) can be Taylor expanded in terms of time derivatives as

$$J^{\mu}(t_0)-\partial_t J^{\mu}(t_0)\vec{n}\cdot\vec{x}'/c+\partial_{tt}J^{\mu}(t_0)(\vec{n}\cdot\vec{x}')^2/(2c^2)+... \tag{3.5.8}$$

only considering the dominant mode $|x|^{-1}$ term in (3.5.6), (3.5.5) can be written in terms of time derivative of current source

$$A^{\mu}=\frac{-|x|^{-1}}{4\pi}\int (J^{\mu}(t_0)-\partial_t J^{\mu}(t_0)\vec{n}\cdot\vec{x}'/c+\partial_{tt}J^{\mu}(t_0)(\vec{n}\cdot\vec{x}')^2/(2c^2)+...)\,dV' \tag{3.5.9}$$

Now in (3.5.9) $\int J^{\mu}(t_0)dV$ the first term is the total charge which is constant. $\int \partial_t J^{\mu}(t_0)\vec{n}.\vec{x}'/c\,dV=\vec{n}.\partial_t\int J^{\mu}\vec{x}'dV'$ second term is derivative of dipole moment which is dominant in electromagnetic radiation. Now we will discuss how this procedure can be extended to gravitational field. Gravitational forces in Newtonian regime satisfies Poisson equation

$$\nabla^2\phi=4\pi G\rho \tag{3.5.10}$$

Now, a 4D variant of above equation has Green's function as general solution

$$\phi(\vec{x},t)=-G\frac{\int \rho(\vec{x}',t-|\vec{x}-\vec{x}'|/c)}{|\vec{x}-\vec{x}'|}dV' \tag{3.5.11}$$

Similar to (3.5.9) power series expansion, (3.5.11) can be written in form of series. $M=\int \rho dV'$ first term in the series is total mass of the system. $\vec{P}=\int \partial_t\rho\vec{x}'_i dV'$ second term is just the total momentum of the system which is also conserved. $\ddot{I}_{ij}=\int \partial_t\rho\vec{x}'_i dV'$ third term is the quadrupole moment which is the first term appears in radiation field. Hence the field potential can be approximated by

$$\phi\approx\frac{-GM}{|\vec{x}|}+\frac{G\vec{n}\cdot\vec{P}}{c|\vec{x}|}-\frac{G\ddot{I}_{ij}n_i n_j}{2c^2|\vec{x}|} \tag{3.5.12}$$

We can only have the only radiative component of (3.5.12) as dimensionless gravitational field

$$h\approx\frac{-G\ddot{I}_{ij}n_i n_j}{2c^4|\vec{x}|} \tag{3.5.13}$$

But to characterize the component of gravitational field which propagates, it has to be transverse and traceless

$$h_{ij} \approx \frac{-G\,\ddot{I}_{ij}\,n_i\,n_j}{2\,c^4|\vec{x}|} \tag{3.5.14}$$

where $I_{ij}=\bar{I}_{ij}-1/3\,\delta_{ij}\,I_{kk}$ trace removed. To estimate how much energy is carried away by these waves we associate the flux (F) with them

$$F=\frac{-1}{4\pi G}(\vec{n}\cdot \mathrm{grad}(\phi))\,\dot{\phi} \tag{3.5.15}$$

In local wave zone, where the $\vec{n}\cdot\mathrm{grad}(\phi)\approx-\dot{\phi}$, the expressions for flux of waves and its respective luminosity are

$$F=\frac{1}{4\pi G}\dot{\phi}^2=\frac{c^3}{4\pi G}\dot{h}^2 \tag{3.5.16}$$

$$L=4\,\pi|\vec{x}|^2\,F \sim (\frac{G}{4\,c^2})\dddot{I}^2 \tag{3.5.17}$$

The expression (3.5.17) for luminosity is a good approximate for the full general relativity result. The rate of energy carried by the waves can be given by expression

$$\frac{dE}{dt}=-\int T^{0r}_{GW}\,dA \tag{3.5.18}$$

where T^{0r}_{GW} is the energy momentum tensor for GW at radial distance r. So in the local wave zone this expression takes form of this famous result

$$\frac{dE}{dt}=-\frac{1}{32\pi}\int\left\langle h^{TT}_{ij}\,h^{TT}_{ij}\right\rangle dA \tag{3.5.19}$$

or

$$\frac{dE}{dt}=-\frac{G}{5\,c^2}\int\left\langle \ddot{I}_{ij}\,\ddot{I}_{ij}\right\rangle dA \tag{3.5.20}$$

3.6 Expansion in Source Region for Slow Motion Sources

The method of multipole expansion can be expanded to the slow motion sources and considering field points far away from the source. By slow motion sources we mean when velocities are negligibly small compared to the speed of light. Such conditions are met by pulsars, where speeds are non-relativistic. Instead of multipole expansion of factor $|\vec{x}-\vec{x}\,'|^{-1}$ we will approximate this as r. Thus, (3.5.11) can now be Taylor expanded in terms of r. The expansion series for the gravitational potential can be given in terms of time derivatives of source mass density

$$\phi = -G \int \frac{1}{r} \sum_{n=0}^{n=\infty} \left(-\frac{r}{c}\right)^n \frac{1}{n!} \frac{d^n}{dt^n} (\rho(\vec{x}', t))\, dV' \tag{3.6.1}$$

We will expand the series and look for the possible dynamical terms in the expansion. The first term is just the Newtonian potential term.

$$\phi_N = -G \int \frac{1}{r} \rho\, dV' \tag{3.6.2}$$

The second term does not contribute either.

$$\frac{G}{c} \int \dot{\rho}\, dV' = \frac{G}{c} \frac{d}{dt} \int \rho\, dV' = 0 \tag{3.6.3}$$

The third term is the first post-Newtonian term.

$$\phi_{PN_1} = \frac{-G}{2c^2} \int r \ddot{\rho}\, dV' \tag{3.6.4}$$

The fourth is a term with a factor of r^2 which suggests it is independent of $\vec{x}$ so it does not contribute either.

$$\frac{G}{3c^3} \int r^2 \dddot{\rho}\, dV' = \frac{G}{3c^3} \int (|\vec{x}|^2 - 2\vec{x} \cdot \vec{y} + |\vec{y}|^2) \dddot{\rho}\, dV' \tag{3.6.5}$$

Fig rce

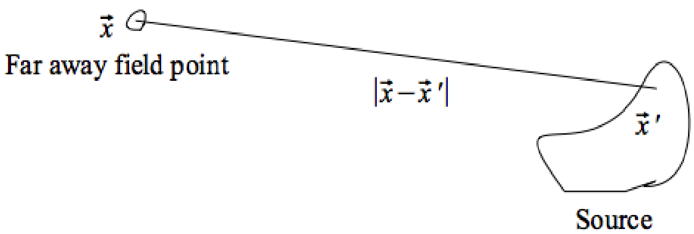

The fifth term is th

$$\phi_{PN_2} = \frac{-G}{c^4 4!} \frac{d^4}{dt^4} \int r^3 \rho\, dV' \tag{3.6.6}$$

At sixth term of the series radiation reaction is seen. This term is referred as 2.5 post-Newtonian term. However, gravitational field h has to be decomposed in terms of both source mass and mass current distributions which is being valid through weak field near zone and local wave zone (see figure 3.8 for description various wave zones). Let $M_0, M_1, M_3 .. S_0, S_1, S_3 ..$ are the mass and current moments of source respectively then schematically in local wave zone, h can be decomposed as

$$h \sim \frac{M_0}{r} + \frac{\dot{M}_1}{r} + \frac{\ddot{M}_2}{r} \ldots \frac{\dot{S}_1}{r} + \frac{\ddot{S}_2}{r} \ldots \tag{3.6.7}$$

where h falls as 1/r

M_0 mass cannot oscillate
$\dot{M}_1$ momentum cannot oscillate
$\ddot{M}_2$ first term is mass quadrupole moment
$\dot{S}_1$ angular momentum cannot oscillate
$\ddot{S}_2$ current quadrupole term is dominant for neutrons stars

Similarly, for the weak field near zone decomposition can given by

$$h \sim \frac{M_0}{r} + \frac{M_1}{r^2} + \frac{M_2}{r^3} \ldots \frac{S_1}{r} + \frac{S_2}{r^2} \ldots \tag{3.6.8}$$

Table 3.2. Comparison of various post-Newtonian terms mentioned with their effects.

Term		Effects
Newtonian		Kepler
PN	$(\frac{v}{c})^2$	Perihelion shift
$P^{1.5}N$	$(\frac{v}{c})^3$	Spin-Orbit coupling (Frame drag)
P^2N	$(\frac{v}{c})^4$	Spin-Spin coupling
$P^{2.5}N$	$(\frac{v}{c})^5$	Radiation reaction

Any gravitational field around a mass source can be categorized into wave generation and wave propagation zones. Thus, dividing the region into zones so that we can be safely apply different set of mathematical tools for both. An inner radius r_I encompassing the wave generation zone (weak field near zone and strong field region) and on the other hand outer radius r_o defining the inner boundary of wave propagation zone (distant wave zone). However, these two zones overlap in local wave zone defined by radius $r_I \leq r \leq r_0$. The inner radius r_I is far away from the source ($r_I \gg \lambda\!\!\!^{-}$) such that gravity of the source is weak. The outer radius r_o is far away from inner one ($r_o - r_I \gg \lambda\!\!\!^{-}$), but not that far away that gravitational redshift and background curvature significantly affect the propagation. Weak field near zone is defined by radius ($2M \ll r \ll \lambda\!\!\!^{-}$) and strong field zone by $r \leq M$. The expansion we have dealt with is valid in the local wave zone and weak field near zone of radiation. The gravity field in strong field zone is so strong in magnitude and non-linear in character that such expansions are not anymore accurate. Numerical treatment of Einstein's equations is the only method which can safely be exploited in strong wave zone. The treatment of numerical relativity for strong zone will be dealt in Chapter 5. The various wave zones around source mass are depicted in figure 3.8.

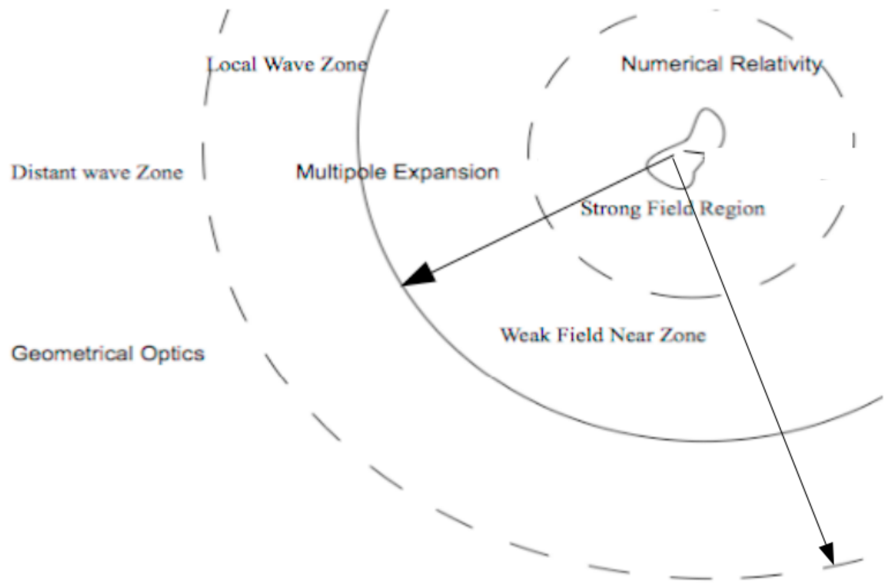

Figure 3.8. Depicting various wave zones around mass source and techniques applied for analysis, see [28,2].

4 Post-Newtonian Approximation

4.1 Post-Newtonian Approximation

The main objective of this section to explore how we can manipulate the post-Newtonian technique to determine the various observables associated with a gravitational wave. The two-body problem we are considering here is black hole binaries, which are inspiralling around the centre of mass. The energy of the system is lost by the outgoing radiation. The gravitational reaction forces the two black holes to come closer and closer into a downward inspiral and eventually merge to form a single black hole resulting in a burst of radiation. In Figure 2.3 various stages of binary black hole coalescence are shown. The purpose of the whole effort is extract waves and compare them with the signals received by the ground base observatories which will assist in accurate understanding the binary black hole problem. This chapter is an adaptation of [4].

The most successful theory of gravitation, general relativity has failed to provide an exact solution to two body problem. Numerical techniques are the only hope for an approximate understanding of binary dynamics. One outstanding technique is the post-Newtonian (PN) approximation in which flux (F) of the gravitational waves is obtained by a series expansion in parameter $v/c=\sqrt{GM/rc^2}$ where v is the source velocity and r(t) *S*chwarzschild radial distance between black holes. The PN approximations are highly successful in obtaining the decay of binary pulsars with the emission of GW [4,6,24]. However binary pulsars don't test the PN theory to highest order as the relativistic velocities of pulsars are small ($v/c\sim 3\times 10^{-3}$). The approximation is valid for the inspiral regime where the parameter is small. Currently these expressions are known up to 3.5 PN order (where v^n corresponds to term of n/2 PN order). The expressions of wave flux F and non-relativistic energy E can be given in terms of series in v

$$E=-\frac{1}{2}\eta v^2\sum_{k=0}^{\infty} E_k v^{2k} \tag{4.1.1}$$

$$F=\frac{32}{5}\eta^2 v^{10}\sum_{k=0}^{\infty} F_k v^k \tag{4.1.2}$$

where $\eta=m_1 m_2/(m_1+m_2)^2$ symmetric mass ratio for binary with masses m_1 and m_2. E_k and F_k (expansion coefficients) are only functions of η. The method assumes adiabatic approximation which insures that the fractional change of orbital velocity over an orbital period is negligibly small ($\Delta\omega/\omega \ll 1$) and luminosity of radiation is proportional to rate of change of orbital frequency. For the circular orbits the energy balance equation is

$$F=-M\frac{dE}{dt} \tag{4.1.3}$$

One would use the following coupled differential equations for the evolution of the orbital phase

$$\frac{d\phi}{dt}-\frac{v^3}{M}=0 \tag{4.1.4}$$

$$\frac{dv}{dt}+\frac{F(v)}{M E'(v)}=0 \tag{4.1.5}$$

where we have used the fact that ϕ (orbital phase) which is the half the gravitational wave phase φ in restricted waveform at dominant order and $v^3=\pi M f$ where f is frequency of GW. Solutions to these ordinary differential equations are

$$t(v)=t_0+M\int_v^{v_0}\frac{E'(v)}{F(v)}dv \tag{4.1.6}$$

$$\phi(v)=\phi_0+M\int_v^{v_0}\frac{E'(v)}{F(v)}v^3 dv \tag{4.1.7}$$

where t_0, ϕ_0 are integration constants, v_0 is a reference velocity and $E'(v)=dE(v)/dv$. All that is left is to estimate the expressions (4.1.6) and (4.1.7) with various orders of F(v) and E'(v) in terms of series and solve the differential equations (4.1.4) and (4.1.5) with numerical techniques. Currently, the expressions for the E(v) and F(v) are known up to 3 PN and 3.5 PN orders respectively.

$$E_{(3)}(v)=-\frac{1}{2}\eta v^2\left[1-\left(\frac{3}{4}+\frac{1}{12}\eta\right)v^2-\left(\frac{27}{8}-\frac{19}{8}\eta+\frac{1}{24}\eta^2\right)v^4+E_3 v^6\right] \tag{4.1.8}$$

$$F_{(3.5)}(v)=\frac{32}{5}\eta^2 v^{10}\left[1-\left(\frac{1247}{336}+\frac{35}{12}\eta\right)v^2-4\pi v^3+F_4 v^4+F_5 v^5+F_6 v^6+F_7 v^6\right] \tag{4.1.9}$$

where expansion coefficients are

$$E_3 = -\left(\frac{675}{64} - \left(\frac{34445}{576} - \frac{205\pi^2}{96}\right)\eta + \frac{155}{96}\eta^2 + \frac{35}{5186}\eta^3\right)$$
$$F_5 = -\left(\frac{8191}{672} + \frac{583}{24}\eta\right)\pi$$
$$F_7 = -\left(\frac{16285}{504} - \frac{214757}{1728}\eta - \frac{193385}{3024}\eta^2\right)\pi$$
$$F_6 = \frac{6643739519}{69854400} + \frac{16}{3}\pi^2 - \frac{1712}{105}\gamma + \left(\frac{41}{48}\pi^2 - \frac{134543}{7776}\right)\eta - \frac{94403}{3024}\eta^2 - \frac{775}{324}\eta^3 - \frac{856}{105}\log(16\,v^2)$$

and $\gamma = 0.577216...$ is the Euler constant.

4.2 TaylorT2

The expression of E'(v)/F(v) in equations (4.1.6) and (4.1.7) has to be truncated up to valid PN order. Evaluating the expressions by integrating them one would obtain the following expressions for 3.5 PN order.

$$\begin{aligned}\phi_{(3.5)}(v) = \phi_0 - \frac{1}{32\eta v^5}[\, & 1 + \left(\frac{3715}{1008} + \frac{55}{12}\eta\right) - 10\pi v^3 + \left(\frac{15293365}{1016064} + \frac{27145}{1008}\eta + \frac{3085}{144}\eta^2\right)v^4 + \\ & \left(\frac{38645}{672} - \frac{65}{8}\eta\right)\ln\left(\frac{v}{v_{lso}}\right)\pi v^5 + \left(\frac{12348611926451}{18776862720} - \frac{160}{3}\pi^2 - \frac{1712}{21}\gamma\right)v^6 + \\ & \left(\left(\frac{2255}{48}\pi^2 - \frac{15737765635}{12192768}\right)\eta + \frac{76055}{6912}\eta^2 - \frac{127825}{5184}\eta^3 - \frac{856}{21}\log(16\,v^2)\right)v^6 + \\ & \left(\frac{77096675}{20321128} + \frac{378515}{12096}\eta - \frac{74045}{6048}\eta^2\right)\pi v^7\,]\end{aligned} \tag{4.2.1}$$

$$\begin{aligned}t_{(3.5)}(v) = t_0 - \frac{5M}{256\eta v^8}[\, & 1 + \left(\frac{743}{252} + \frac{11}{3}\eta\right)v^2 - \frac{32}{5}\pi v^3 + \left(\frac{3058673}{508032} + \frac{5429}{504}\eta + \frac{617}{72}\eta^2\right)v^4 + \\ & \left(\frac{7729}{252} - \frac{13}{3}\eta\right)\pi v^5 + \left(-\frac{1052469856691}{2347107840} + \frac{128}{3}\pi^2 + \frac{6848}{105}\gamma + \left(\frac{3147553127}{3048192} - \frac{451}{12}\pi^2\right)\eta\right)v^6 \\ & \left(-\frac{15211}{1728}\eta^2 + \frac{25565}{1296}\eta^3 + \frac{3424}{105}\log(16\,v^2)\right)v^6 + \left(-\frac{15419335}{127008} - \frac{75703}{756}\eta + \frac{14809}{378}\eta^2\right)\pi v^7\,]\end{aligned} \tag{4.2.2}$$

Both expressions have transcendental functions which require lot of computation power for obtaining high resolution waveforms. For simulation purposes, t_0 can be chosen to be time of coalescence for binaries. By reverting (4.2.2) the expression, v(t) can be found by determining roots of polynomial of v for a given time interval.

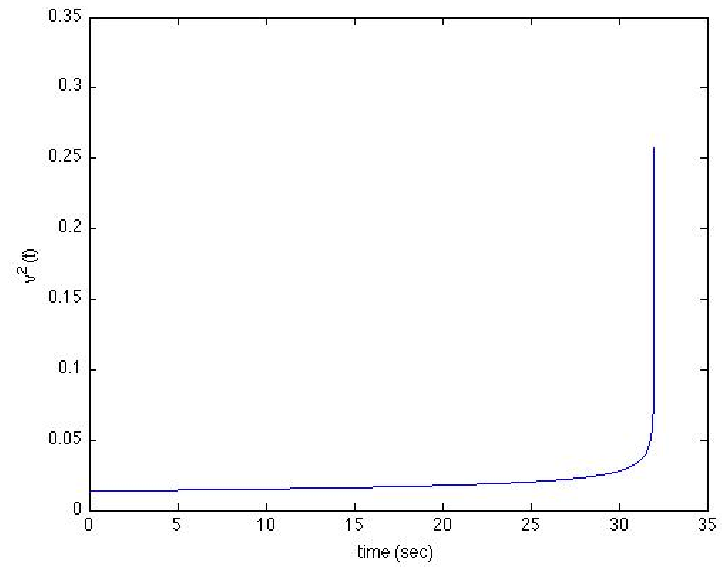

Figure 4.1. The $v(t)^2$ is extracted by reverting the expression (4.2.2) and finding the roots for given time interval, considering it as a polynomial in $v(t)^2$. Here time for coalescence is 32s for $M_{\Theta}=1.4$ binaries. The $v(t)^2$ represents a much accurate description of amplitude of gravitational waveforms.

4.3 TaylorT3

As shown in section 4.2 by finding the explicit expression for $\phi(v)$ and $t(v)$ one would revert the expression (4.2.2) and can determined $\phi(v(t))$. The equations for orbital phase and instantaneous frequency of GW for 3.5 PN then can obtained as

$$\begin{aligned}\phi_{(3.5)}(t)=\phi_0-\frac{1}{\eta\theta^5}[&\left(\frac{3715}{8064}+\frac{55}{96}\right)\theta^2-\frac{3}{4}\theta^3+\left(\frac{9275495}{14450688}+\frac{284875}{258048}+\eta+\frac{1855}{2048}\eta^2\right)\theta^4+\left(\frac{38645}{21504}-\frac{65}{256}\eta\right)\ln\left(\frac{\theta}{\theta_{lso}}\right)\pi\theta^5\\ &+\left(\frac{831032450749357}{57682522275840}-\frac{53}{40}\pi^2+\left(\frac{-126510089885}{4161798144}+\frac{2255}{2048}\pi^2\right)\eta-\frac{107}{56}\gamma+\frac{154565}{1835008}\eta^2\right)\theta^6\\ &+\left(\frac{-1179625}{1769472}\eta^3-\frac{107}{56}\log(2\theta)\right)\theta^6+\left(\frac{-189516689}{433520640}-\frac{97765}{258048}\eta+\frac{141769}{1290240}\eta^2\right)\pi\theta^7]\end{aligned}\tag{4.3.1}$$

$$\begin{aligned}f_{(3.5)}=\frac{\theta^2}{8\pi M}[&1+\left(\frac{743}{2688}+\frac{11}{32}\eta\right)\theta^2-\frac{3}{10}\pi\theta^3+\left(\frac{1855099}{14450688}+\frac{56975}{258048}\eta+\frac{371}{2048}\eta^2\right)\theta^4-\left(\frac{7729}{21504}-\frac{13}{256}\eta\right)\pi\theta^5\\ &\left(\frac{720817631400877}{288412611379200}+\frac{53}{200}\pi^2+\frac{107}{280}\gamma+\left(\frac{25302017977}{416178144}-\frac{451}{2048}\pi^2\right)\eta-\frac{30913}{1835008}\eta^2\right)\theta^6+\\ &\left(\frac{235925}{1769472}\eta^3+\frac{107}{280}\log(2\theta)\right)\theta^6+\left(-\frac{188516689}{433520640}-\frac{97756}{258048}\eta+\frac{141769}{1290240}\eta^2\right)\pi\theta^7]\end{aligned}\tag{4.3.2}$$

where $\theta=\left(\eta\left(t_0-t\right)/5M\right)^{-1/8}$ and $f\equiv(2\phi')(2\pi)^{-1}=v^3/\pi M$. Given value of t_0 one can find orbital phase and frequency of gravitational waves. As $t\rightarrow t_0$ frequency $(F(t))$ diverges.

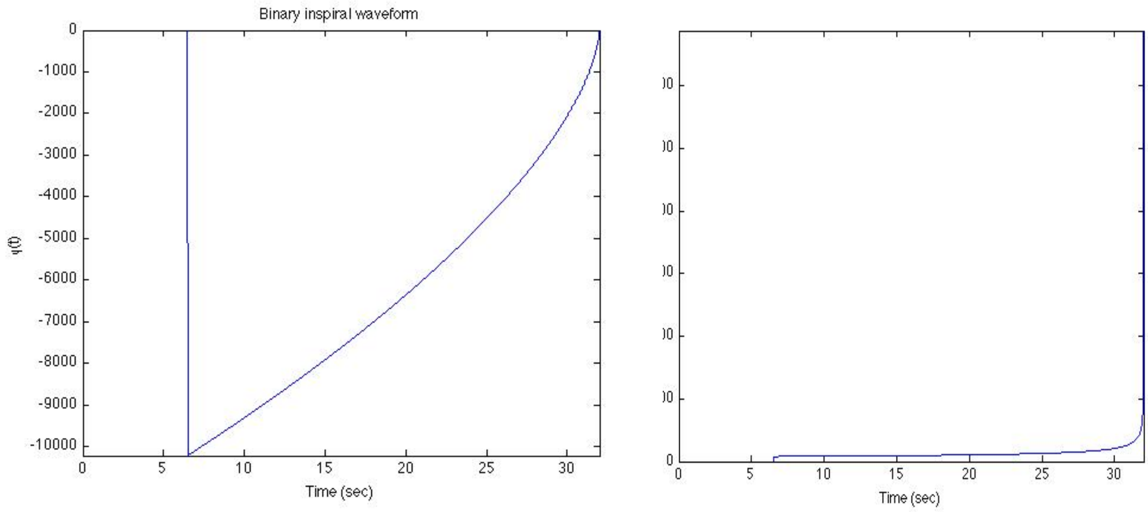

Figure 4.2. The instantaneous phase ($\varphi(t)$) and frequency ($F(t)$) of gravitational wave for $M_{\Theta}=1.4$ binaries with $t_0=32\sec$ are shown. The order of instantaneous phase was truncated up to θ^4 term. It's evident that $F(t)$ diverges at $t \rightarrow t_0$.

4.4 Extraction of Binary Inspiral Waveforms

The inspiral waveforms can be extracted by the expression

$$h(t)=A_p\cos(2\phi(t))+A_c\sin(2\phi(t)) \tag{4.4.1}$$

where A_c, A_p and are the amplitude of cross-polarised and plus polarised GW. The expression for $\phi_{(3.5)}(t)$ was truncated up to θ^4 term. The amplitude, A(t) is given by the response of antenna to the gravitational wave as given by expression

$$A(t)=\frac{4CM_C}{D_L}(\pi M_c f_{GW}(t))^{\frac{2}{3}} \tag{4.4.2}$$

where $M_C=\eta^{3/5}(m_1+m_2)$, D_L is the luminosity distance, C ($0 \le C \le 1$) is geometric factor that depends on the orientation angle between antenna and binary system. By (4.4.2) explicit expressions for A_c and A_p can be determined as

$$A_c(t)=\frac{-2CM_C}{D_L}(2\cos(i))(\pi M_c f_{GW}(t))^{\frac{2}{3}} \tag{4.4.3}$$

$$A_p(t)=\frac{-2CM_C}{D_L}(1+\cos(i)^2)(\pi M_c f_{GW}(t))^{\frac{2}{3}} \tag{4.4.4}$$

where *i* is the inclination angle of binary with earth.

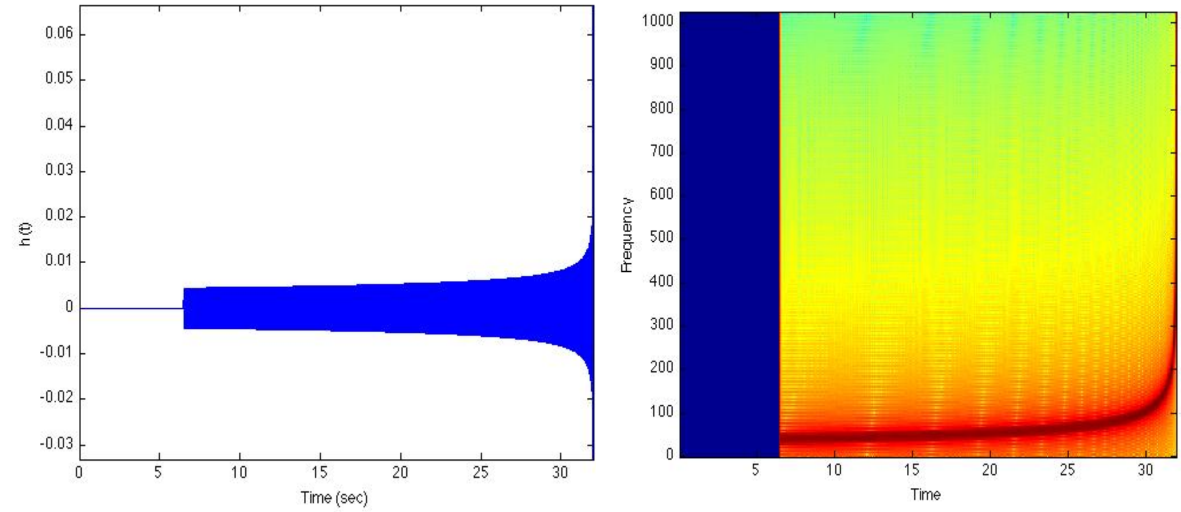

Figure: 4.3. Gravitational waveform for $M_{\Theta}=1.4$ binaries with $t_0=32\sec$ and $i=0$ is shown. The waveform were extracted by (4.4.1) considering C as unity. It's evident from spectrogram that the frequency diverges as time of coalescence is reached.

Another more realistic way to extract waveform is by exploiting the expression

$$h(t)=v(t)^2\cos(2\phi(t)) \tag{4.4.5}$$

which is a much more accurate description of GW amplitude in comparison to above method. The reason for being such a nice waveform is that amplitude varies dominantly proportional to $v(t)^2$. The results for such waveform are shown in Figure 4.4.

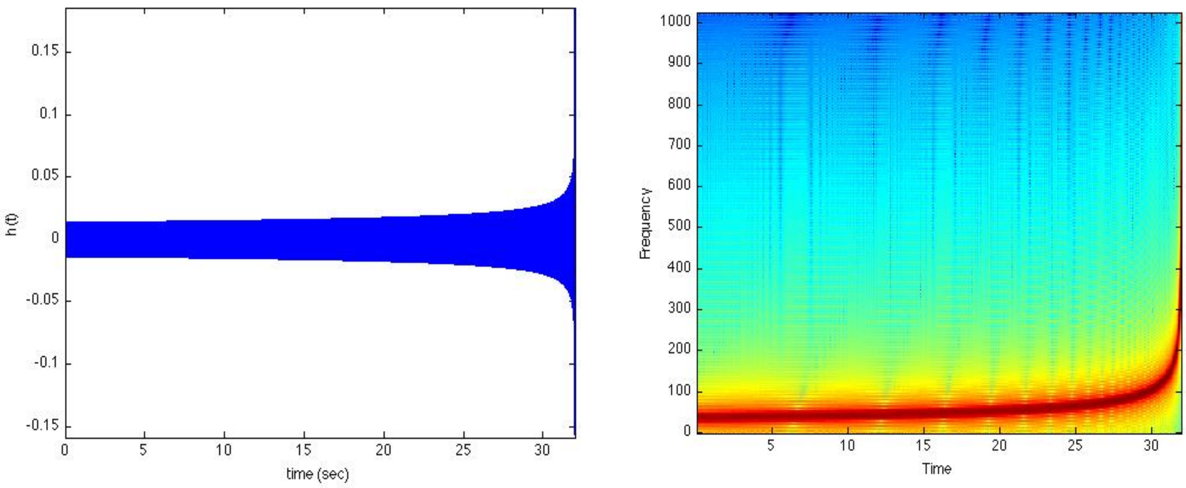

$$h(t)=A(t)\cos(\varphi(t)) \tag{4.5.1}$$

where A(t) is given by (4.4.2). The purpose of neglecting amplitude corrections simplifies the process of data analysis to a large extent. For our purposes, Fourier domain is a good choice to work with, Fourier transform of (4.5.1) yields

$$\tilde{h}(f)=A(t)\int_{-\infty}^{+\infty} e^{2\pi i f t}\left(e^{-i\varphi(t)}+e^{i\varphi(t)}\right)dt=A(t)\int_{-\infty}^{+\infty}\left(e^{i(2\pi f t-\varphi(t))}+e^{i(2\pi f t+\varphi(t))}\right)dt \qquad (4.5.2)$$

expression (4.5.2) can be dealt with as stationary phase approximation. It's the far most popular way of extracting the waveforms, the approximation yields

$$\tilde{h}(f)=\frac{C}{D_L\pi^{2/3}}\frac{\sqrt{5}}{24}(M_C)^{\frac{5}{6}}e^{i\Psi(f)+i\frac{\pi}{4}} \qquad (4.5.3)$$

where

$$\Psi(f)=2\pi f\, t_0+\Phi_0+\sum_{k=0}^{7}\psi_k f^{(k-5)/3} \qquad (4.5.4)$$

and the expansion coefficients for $\Psi(f)$ in (4.5.4) are given by

$$\psi_k=\frac{3}{128\mu}(\pi M)^{(k-5)/3}\alpha_k$$

$$\alpha_0=1,\ \alpha_1=0,\ \alpha_2=\frac{3715}{756}+\frac{55}{9}\eta,\ \alpha_3=-16\pi,\ \alpha_4=\frac{15293365}{508032}+\frac{27145}{504}\eta+\frac{3085}{72}\eta^{2,}$$

$$\alpha_5=\pi\left(\frac{38645}{756}-\frac{65}{9}\eta\right)\left(1+\ln(6^{3/2}\pi M f)\right)$$

$$\alpha_7=\pi\left(\frac{77096675}{254016}+\frac{378515}{1512}\eta-\frac{74045}{756}\eta^2\right)$$

$$\alpha_6=\frac{11583231236531}{4694215680}-\frac{640}{3}\pi^2-\frac{6848}{21}\gamma+\left(\frac{-15737765635}{3048192}+\frac{2255}{12}\pi^2\right)\eta+\frac{76055}{1728}\eta^2-\frac{127825}{1296}\eta^3-\frac{6848}{63}\ln(64\pi M f)$$

The coefficients α_5 and α_6 are not constant as they have *log f*-dependence but we can treat them as constant if we assume that *log f*-dependence is weak in the desired bandwidth. For simulations the expression for $\Psi(f)$ was evaluated up to k=2.

However, computations as suggested by (4.5.3) produce some artifacts (spurious frequencies). These artifacts has to be removed by truncating frequencies greater then f_0 . To produce the required waveform in time domain inverse Fourier transform has to be performed which again generate some false frequencies in waveform. Bandpass filtering has to be performed to throw away some of lowest and highest false frequencies. The results are shown in figure 4.5.

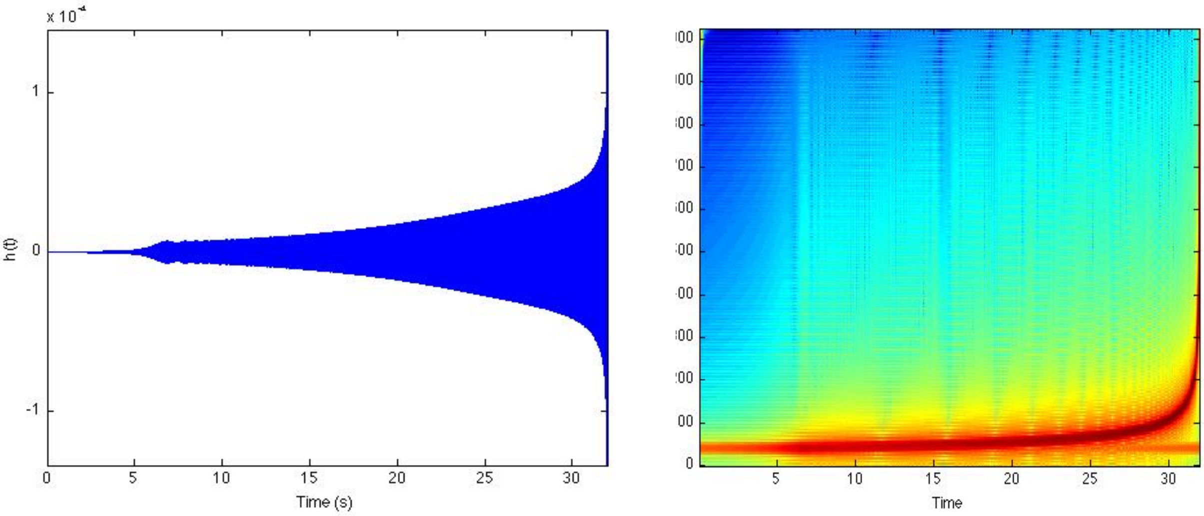

Figure 4.5. The waveform was extracted by the stationary phase approximation procedure described in this section. The waveform are obtained for $M_{\Theta}=1.4$ binaries with $t_0 = 32$ s.

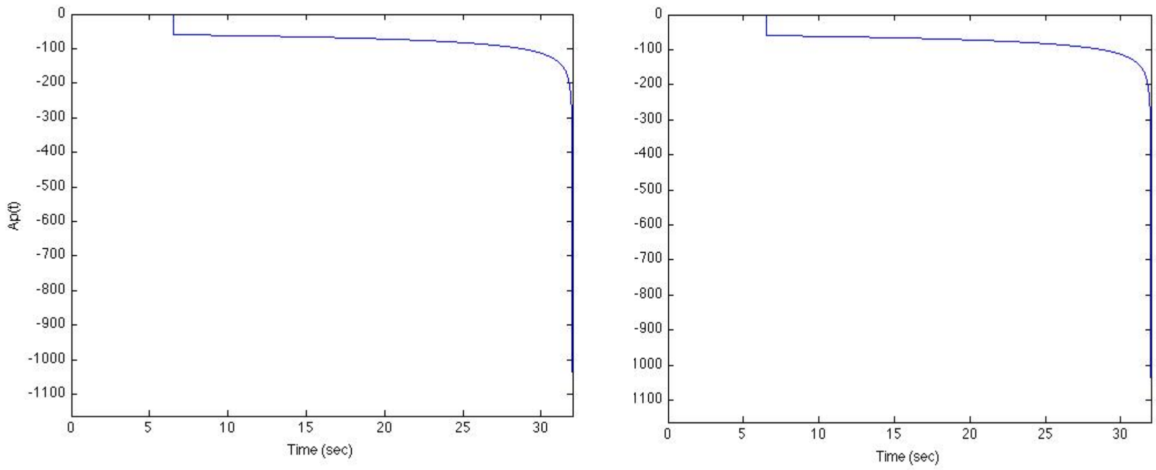

Figure 4.7 (a). Amplitude of cross and plus polarised gravitational wave at *i*=0

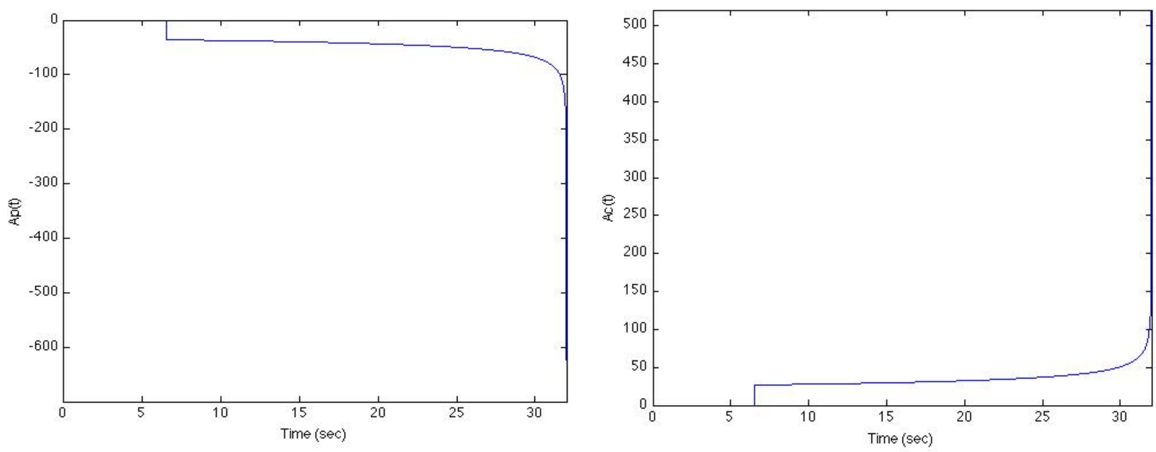

Figure 4.7 (b). Amplitude of cross and plus polarised gravitational wave at *i*=90

5 Numerical Relativity

In general relativity the two-body problem is of special interest. The binary black hole problem has become exciting and challenging in astrophysics. On the successful operation of detectors all around the world, interest is growing on receiving signals from supernovae bursts, star collapse and binary black holes coalescence. But one major issue with GW is its complexity to extract waveform and weakness of received signal. Numerical relativity plays a vital role to extract waveforms from background noise by matching with already existing waveforms banks. The interest is growing due to the exponential increase in computational power of clusters over the past decades. The binary black hole in vacuum are the primary sources of gravitational radiation. We already have discussed briefly various phases of the binaries resulting in signature waveforms. Post-Newtonian approximation is one the effort to solve the issue. But this method has its own limitations in strong gravitational interactions and at relativistic speeds. The sole purpose of numerical relativity is to solve Einstein's equations by numerical techniques for various astrophysical scenarios. The final stages of black hole coalescence involve strong gravitational interactions where only numerical relativity methods are valid. Post-Newtonian approximations are not useful at such extreme curvatures and relativistic speeds.

In 1964, the first attempts to solve Einstein's equations by numerical techniques were reported. But at that time the computational resources needed to solve the problem were inadequate. Now we have the computational power and memory to solve the Einstein's equations computationally. Advance algorithms for solving such complex problems has been developed over decades. Our interest in numerical relativity is to extract waveforms from binary black hole evolution and form a template bank which can be utilize to matched with the received signals. Due the technological advancement in supercomputers, this field is becoming increasing mature and lot of previous problems are reconsidered. Collision of axisymmetric black holes, binary black hole inspiral, and coalescence of black hole with initial spin and momentum are being studied. The evolution times are being enough to extract the gravitational waveform. However the simulations of binary black holes space-time turn out to be much more complicated due to the computational challenges they pose.

Einstein's equations can be considered as ten coupled non-linear partial differential equations. The equations can have many equivalent forms. In harmonic form, the metric tensor forms wave equations which are mathematically known for their stability properties. The metric tensor cannot be decomposed into background and perturbations for strong gravity scenarios. Therefore, numerical solution to Einstein's equations is the way forward. There are only six components to be solved for metric the rest of four components are just gauge freedom. The 3+1 split of metric tensor is the basis for the ADM formalism. The BSSN formalism is the conformal modification to this formalism. BSSN has developed interest in the two-body problem because of the stability of evolution on supercomputers. Dealing with space-time singularities is another issue which is to be resolved by method of excision. Excision is accomplished by excluding space points which are causally disconnected but this method comes with a price. Keeping track of apparent horizons at each time step to perform excision is computationally expensive. The excision can be avoided by using puncture initial data for evolution. We will systematically discuss some of the formalism, initial data and findings in this chapter. This chapter is based on systemic study of [1,8,9,10,11,13,14,15,16,17,18,19,26].

5.1 Arnowitt-Deser-Misner (ADM) Formulation

The 3+1 split of Einstein's equations is the most widely used formulation in numerical relativity. Space-time is foliated by considering spacelike hypersurfaces which evolve with coordinate time. So the four-dimensional space-time is split into three-dimensional hyper-surfaces plus time. The idea was first suggested by Arnowitt, Deser and Misner when they were trying to quantize gravity. The technique we will discuss is Cauchy approach which sees space-time as three dimensional space at particular instant of time. To grasp the concept we will first consider 3+1 split of Maxwell's equations. The famous Maxwell's equations can be written in terms of vector potential $\vec{A}$ a set of three equations

$$\nabla\cdot\vec{E}=4\pi\rho \tag{5.1.1}$$

$$\frac{\partial\vec{A}}{\partial t}+\vec{E}+\nabla\phi=0 \tag{5.1.2}$$

$$\frac{-\partial\vec{E}}{\partial t}+\nabla\times\nabla\times\vec{A}=4\pi\vec{J} \tag{5.1.3}$$

The above set of equations can be categorized into two. The ones which are constrained and the ones which are evolution equations. (5.1.1) is a constraint equation which cannot be violated at any instant of time as the evolution continues. (5.1.2) and (5.1.3) are the evolution equations which determines the evolution of fields as time progress. However if the evolution is performed numerically then it cannot be guaranteed that the constraint equations will not be violated.

Now we will continue to 3+1 split of Einstein's equations. The four-dimensional space-time is foliated by three-dimensional hyper-surfaces Σ which are labelled by t. n^{ν} is a normal vector on hyper-surface which points in increasing value of time. We can define a projection tensor $P_{\mu\nu}$ which projects any vector to spatial the hyper-surface Σ. Following are the straight forward properties of such a tensor

$$P_{\mu\nu} \equiv g_{\mu\nu} - n_\mu n_\nu \tag{5.1.4}$$

$$P_{\mu\nu} = P_{\nu\mu} \tag{5.1.5}$$

$$P_{\mu\nu} n^\mu = 0 \tag{5.1.6}$$

The $P_{\mu\nu}$ must be symmetric and should be purely spatial as indicated by (5.1.6). Now projecting the metric tensor to the hyper-surface we will have our spatial metric.

$$\gamma_{ij} = P^\mu_i P^\nu_j g_{\mu\nu} \tag{5.1.7}$$

The projections of time coordinate can be split into spatial direction and part orthogonal to it.

$$\beta^i = P^i_\nu t^\nu \tag{5.1.8}$$

$$\alpha = n_\nu t^\nu \tag{5.1.9}$$

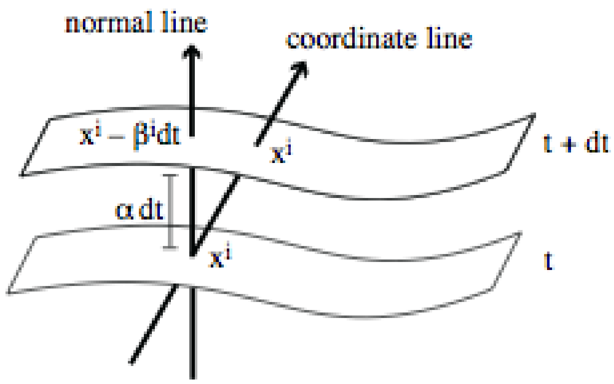

Figure 5.1. Shows the two hyper-surfaces separated by coordinate time dt. The normal line show the direction of future pointing normal vector n^μ. The coordinate line shows the same coordinate on the two hyper-surfaces.

Therefore by (5.1.8) and (5.1.9) we have

$$t^\mu = \alpha n^\mu + \beta^\mu \tag{5.1.10}$$

where α is lapse function which measure the proper time and β^{μ} is shift vector measuring velocity of spatial coordinate labels. Now in terms of spatial metric, lapse function and shift vector whole metric can be written in the form

$$ds^2=-(\alpha\, dt)^2+\gamma_{ij}(dx^i+\beta^i dt)(dx^j+\beta^j dt) \tag{5.1.11}$$

Another important quantity which needed to be defined for ADM formulation is extrinsic curvature. Defined as projecting the covariant derivative of normal vector

$$K_{ij}=P_i^{\mu}P_j^{\nu}D_{\nu}n_{\mu} \tag{5.1.12}$$

Another useful definition for extrinsic curvature is the Lie derivative with normal vector of spatial metric

$$K_{ij}=-\frac{1}{2}L_n\gamma_{ij} \tag{5.1.13}$$

By help of above defined quantities we are now in a position to split the Einstein's equations to formulate ADM equations

$$R^{(3)}+K^2-K_{ij}K^{ij}=16\pi G\rho \tag{5.1.14}$$

$$D_j(K^{ij}-\gamma^{ij}K)=8\pi G j^i \tag{5.1.15}$$

$$\frac{d}{dt}\gamma_{ij}=-2\alpha K_{ij} \tag{5.1.16}$$

$$(\frac{d}{dt}-L_{\vec{\beta}})K_{ij}=-D_iD_j\alpha+\alpha(R_{ij}^{(3)}+K K_{ij}+2K_{il}K_j^l+8\pi[S_{ij}-\frac{1}{2}(S-\rho)]) \tag{5.1.17}$$

where $L_{\vec{\beta}}$ is Lie derivative with respect to β^i, $R^{(3)}$ is the curvature tensor formed by 3D spatial metric, D_i is the covariant derivative, ρ is energy density, j^i is the momentum density, S_{ij} stress energy tensor of matter and K is the trace of K_{ij}. Again (5.1.14) and (5.1.15) are hamiltonian and momentum constraint equations. Whereas (5.1.16) and (5.1.17) are evolution equations for spatial metric and extrinsic curvature respectively. It's always guaranteed by Bianchi identities that a initial solution to constrained equations will always be a solution to evolution equations at later times.

5.2 Baumgarte-Shapiro-Shibata-Nakamura (BSSN) Formulation

The ADM was considered as standard formulation for numerical relativity simulations until recently. As this formulation has some serious issues during the simulation. Evolution with ADM formulation proved to be numerically unstable. Simulation with shorter evolution time were reported. As the system approaches singularity in shorter time, numerical code crashes. BSSN reformulates the evolutions equations (5.1.16) and (5.1.17). This formulation has added advantage of stability and longer simulation times. The basic idea behind this formulation is to split the conformal and traceless part of the ADM evolution equation. This is achieved by introducing new spatial metric $\tilde{\gamma}_{ij}$

$$\tilde{\gamma}_{ij} = e^{-4\phi} \gamma_{ij} \tag{5.2.1}$$

to fix the determinant of metric to unity we have defined the following constrain

$$e^{-4\phi} = \gamma^{1/3} \tag{5.2.2}$$

Instead of using extrinsic curvature we will consider its traceless part A_{ij} which is defined as

$$A_{ij} = K_{ij} - \frac{1}{3}\gamma_{ij} K \tag{5.2.3}$$

Similar to conformal decomposition of spatial metric γ_{ij}, A_{ij} can be decomposed as

$$\tilde{A}_{ij} = e^{-4\phi} A_{ij} \tag{5.2.4}$$

The evolution equation (5.1.17) can be used to find trivial expression for conformal spatial metric $\tilde{\gamma}_{ij}$ and its conformal factor ϕ as

$$\frac{d}{dt}\tilde{\gamma}_{ij} = -2\alpha \tilde{A}_{ij} \tag{5.2.5}$$

$$\frac{d}{dt}\phi = -\frac{1}{6}\alpha K \tag{5.2.6}$$

To find evolution equation for K, expression (5.1.17) can be used, with the aid of hamiltonian constraint (5.1.14) the Ricci scalar is eliminated.

$$\frac{d}{dt}K = -\gamma^{ij} D_i D_j \alpha + \alpha \left[\tilde{A}_{ij} \tilde{A}ij + \frac{1}{3}K^2 + \frac{1}{2}(\rho + S) \right] \tag{5.2.7}$$

For the evolution equation of trace-free part of extrinsic curvature some manipulation of (5.1.17) results in

$$\frac{d}{dt}\tilde{A}_{ij} = e^{-4\phi} \left[-D_i D_j \alpha + \alpha (R_{ij} - S_{ij}) \right]^{TF} + \alpha (K \tilde{A}_{ij} - 2 \tilde{A}_{il} A^l_j) \tag{5.2.8}$$

Due to the conformal decomposition of the spatial metric the Ricci tensor can also be decomposed into conformal part and conformal factor as

$$R_{ij} = \tilde{R}_{ij} + R^{\phi}_{ij} \tag{5.2.9}$$

The conformal factor R^{ϕ}_{ij} can be readily calculated by covariant derivatives of ϕ as

$$R^{\phi}_{ij} = -2\tilde{D}_i \tilde{D}_j \phi - 2\tilde{\gamma}_{ij} \tilde{D}^l \tilde{D}_l \phi + 4\tilde{D}_i \phi \tilde{D}_j \phi - 4\tilde{\gamma}_{ij} \tilde{D}^l \phi \tilde{D}_l \phi \qquad (5.2.10)$$

The conformal part $\tilde{R}_{ij}$ can be computed by the standard conformal spatial metric $\tilde{\gamma}_{ij}$. To simplify matters, we need to define a new variable, conformal connection function as

$$\tilde{\Gamma}^i \equiv \tilde{\gamma}^{jk} \tilde{\Gamma}^i_{jk} = -\tilde{\gamma}^{ij}_{,j} \qquad (5.2.11)$$

Now in terms of conformal connection $\tilde{\Gamma}^i$, Ricci tensor can be written

$$\tilde{R}_{ij} = -\frac{1}{2}\tilde{\gamma}^{lm}\tilde{\gamma}_{ij,lm} + \tilde{\gamma}_{ki}\partial_j \tilde{\Gamma}^k + \tilde{\Gamma}^k \tilde{\Gamma}_{(ij)k} + \tilde{\gamma}^{lm}\left(2\tilde{\Gamma}^k_{l(i}\tilde{\Gamma}_{j)km} + \tilde{\Gamma}^k_{im}\tilde{\Gamma}_{klj}\right) \qquad (5.2.12)$$

Conformal connection function $\tilde{\Gamma}^i$ must be promoted to independent variable as we want the expression (5.2.12) of Ricci tensor to maintain its elliptic behaviour. However this comes with a price of computing three new evolution equations in the formulation. Assuming $\tilde{\Gamma}^i$ as independent variable the equation for its evolution can be given by

$$\frac{\partial}{\partial t}\tilde{\Gamma}^i = -\frac{\partial}{\partial x^j}\left(2\alpha \tilde{A}^{ij} - 2\tilde{\gamma}^{m(j}\beta^{i)}_{,m} + \frac{2}{3}\tilde{\gamma}^{ij}\beta^l_{,l} + \beta^l \tilde{\gamma}^{ij}_{,l}\right) \qquad (5.2.13)$$

Still the above expression has stability issues when numerical simulations are done. The situation can be improved by removing the divergence of $\tilde{A}^{ij}$ with the help of momentum constraint (5.1.16).

$$\frac{\partial}{\partial t}\tilde{\Gamma}^i = -2\alpha \tilde{A}^{ij}\alpha_{,j} + 2\alpha\left(\tilde{\Gamma}^i_{jk}\tilde{A}^{kj} - \frac{2}{3}\tilde{\gamma}^{ij}K_{,j} - \tilde{\gamma}^{ij}S_j + 6\tilde{A}^{ij}\phi_{,j}\right) - \frac{\partial}{\partial x_j}\left(\beta^l \tilde{\gamma}^{ij}_{,l} - 2\tilde{\gamma}^{m(j}\beta^{i)}_{,m} + \frac{2}{3}\tilde{\gamma}^{ij}\beta^l_{,l}\right)$$

(5.2.14)

With this the evolution structure of BSSN is complete. The evolutions equations for $\phi, K, \tilde{A}_{ij}$, and $\tilde{\Gamma}^i$ represents complete set of equations. The new formulation is much more stable as the equations are well posed and have strong hyperbolicity.

5.3 Boundary Conditions

The computational domain of numerical relativity does not cover the whole space-time to spatial infinity due to lack of computational resources. Moreover, the domain covered by such simulation is pretty small such that boundary lies right where the space-time is dynamic. Therefore suitable boundary condition must be provided so to minimize the reflection and outgoing waves leave the boundary smoothly. Such boundary must be set so that there are not artificial reflection and boundary conditions cause no instability. But this issue is not as simple as it seems due to several reasons. All dynamical variables do not behave as waves at such distances which are set by computational domain for simulations. Secondly, there are no local boundary conditions which are provided for the incoming wave to leave the grid cleanly. We will now briefly discuss the boundary conditions (that can be set in Cactus (see section 5.6 for details)) for binary black hole space-times.

Static Boundary Condition: By static we mean that at boundary no dynamical variable is updated and they retain their initial values throughout the evolution. This condition is does the worse in our case and introduces lot of artificial reflection of gravitational waves. However the condition may suit such scenarios where static condition are required at boundary to avoid truncation errors.

Flat Boundary Condition: Flat boundary condition allows some dynamics at the boundary as compare to static condition but still introduces significant amount of reflections. When flat boundary is set the boundary value is just copied from a interior point where dynamical variable are calculated. Still this condition does no good for our purpose.

Radiative Boundary Condition: This boundary serves the purpose for a clean outlet of waves from the grid. It assumes that dynamical variable behaves like constant (f_0) plus outgoing radial wave which decays as 1/r at the boundary of the grid.

$$f(\vec{x},t)=f_0+u\frac{(r-t)}{r} \tag{5.3.1}$$

where $r=\sqrt{(x^2+y^2+z^2)}$, and f_0 is taken to one of diagonal elements of metric and rest are zero. The expression (5.3.1) clearly shows that we are assuming that outgoing waves behaves like smooth wavefronts at the boundary. This boundary condition has found to be very useful for avoiding artificial reflections. However, there is more to it, to implement (5.3.1) its differential form (5.3.2) is more useful in practice. As differential equations can be implemented as difference in equations by numerical techniques.

$$\frac{x_i}{r}\partial_t f+\partial_i f+\frac{x_i}{r^2}(f-f_0)=0 \tag{5.3.2}$$

5.4 Gauge Conditions

The possible values of lapse and shift are one of the gauge choices which are needed to be provided before the evolution. For gauge conditions we concentrate on the lapse function only because shift vector is often chosen to be zero for our purpose. Determining the value for lapse function can be done in to three ways.

Prescribed Slicing: Specify the lapse initially for a given space-time by the known a prior conditions. The simplest example of such gauge is geodesic slicing. Gauge choice for geodesic slicing is

$$\alpha\equiv 1 \quad \text{and} \quad \beta\equiv 0 \tag{5.4.1}$$

The gauge choice simply suggests that it follows time-like geodesic with proper time of Eulerian observer. The geodesic slicing allows very short evolution times as coordinate singularity is achieved at quite early stage. Like for Schwarzschild initial data singularity is achieved at πM time. Shorter simulation times covers very small space-time domain thus extraction of gravitational wave is not possible which is not desirable.

Elliptic Slicing: This the most robust and accurate of form of slicing condition. Usually lapse is determined by solving elliptic differential equation on each time step by imposing some condition on the spatial hyper-surfaces. However, solving elliptic equation on each time step is a computationally expensive task.

Algebraic Slicing: The slicing calculates lapse and its time derivative on each hyper-surface as a function of spatial metric and extrinsic curvature. The slicing condition can be computationally cheap. However it's difficult to analyse data analytically. The most common used type of such gauge is hyperbolic K-driver condition. The lapse function is readily calculated by

$$(\partial_t - L_{\vec{\beta}})\alpha = -\alpha^2 F(\alpha) K \tag{5.4.2}$$

The main advantages of such slicing condition is that it's cheap and lapse decays to zeros in regions of strong curvature. The typical choice for $F(\alpha)$ is $2/\alpha$ which is known as 1+log slicing. 1+log slicing the far most commonly used condition. It's cheaper for computers then elliptic slicing condition and moreover foliates the action of singularity avoidance.

5.5 Initial Data for Black Hole

As we have developed suitable formulation for the evolution of black hole space-time and have seen the constraint equations the natural question will be, which space-times satisfies such initial conditions and evolve with stability. To simplify the matters we are assuming that extrinsic curvature K_{ij} is set to zero. This condition simplifies matters a lot. Such assumption makes the momentum constraint trivial, however the hamiltonian constraint still needs to solved. The requirement is that we want black hole to exist on initial hyperspace which eventually evolve at time progress. For purpose of solving hamiltonian constraint our assumption is that spatial metric $\tilde{\gamma}^{ij}$ is flat. This leads to simplification of hamiltonian constraint as

$$\tilde{D}^2 \psi = 0 \tag{5.5.1}$$

where the $\tilde{D}$ covariant derivative associated conformal spatial metric $\tilde{\gamma}^{ij}$. Solution to (5.5.1) leads to Schwarzschild and Misner initial data.

5.5.1 Schwarzschild Initial Data

Schwarzschild solved the Einstein's equations for a spherical symmetric vacuum space-time. The solution represents the exterior of a star or a black hole.

$$ds^2 = -\left(1-\frac{2M}{r_s}\right)dt_s^2 + \frac{1}{\left(1-\frac{2M}{r_s}\right)}dr_s^2 + r_s^2 d\theta^2 + r_s^2 \sin\theta^2 d\phi^2 \tag{5.5.2}$$

The metric is a static solution to Einstein's equations as given in Schwarzschild coordinates (t_s, r_s, θ, ϕ). To avoid the coordinate singularity, we can choose isotropic radial coordinate which is related to radial coordinate as

$$r_s = \left(1+\frac{M}{2r}\right)^2 r \tag{5.5.3}$$

The Schwarzschild metric in isotropic coordinates is given as

$$ds^2 = -\left(\frac{2r-M}{2r+M}\right)^2 dt^2 + \left(1+\frac{M}{2r}\right)^4 (dr^2 + r^2 d\Omega^2) \tag{5.5.3}$$

where $d\Omega^2 = d\theta^2 + \sin^2\theta\, d\phi^2$. The spatial metric and conformal factor are set to following values

$$\tilde{g}_{ij} = \psi^4 \delta_{ij} \tag{5.5.4}$$

$$\psi = \left(1+\frac{M}{2r}\right) \tag{5.5.5}$$

For simulation purposes black hole resides at the origin of the grid. The isotropic lapse function has value $2r-M/2r+M$ which can be set by using proper parameters in Cactus. However, isotropic lapse function retain its initial value throughout the evolution. The evolution of Schwarzschild initial data can be treated as primary step to evolve more complex systems, like coalescence of two black holes. Previously, this problem has been treated numerically to gain experience for binary systems [18,19].

5.5.2 Misner Initial Data

In 1960, Misner proposed a way to represent space-time of two black holes. The solution can be generalized to any number of black holes [17]. The metric represents two non-rotating black holes momentarily at rest and their throats are connected by two wormholes as show in figure 5.2. The two throats connected two asymptotic flat space-times. The throats can be thought as apparent horizons of black holes. The general metric for Miner data is given as

$$ds^2 = -dt^2 + \psi^4 (dx^2 + dy^2 + dz^2) \tag{5.5.6}$$

The conformal factor has the following solution to hamiltonian constraint for two throat data

$$\psi = \sum_{n=-\infty}^{+\infty} \frac{1}{\sinh(\mu_0 n)} \frac{1}{\sqrt{x^2 + y^2 + (z + \coth(\mu_0 n))^2}} \tag{5.5.7}$$

However in practice the summation is cutoff to n =30, which is being tested for applications and works very well. The relations are given in cylindrical coordinates ((r, θ, z)).

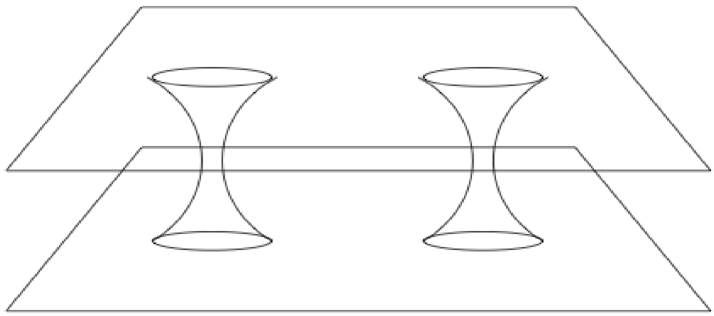

Figure 5.2. The asymptotic flat regions are connected by two Einstein-Rosen bridges or wormholes representing the two black holes. Clearly, an isometry is there between upper and lower half of the two bridges.

μ_0 determines the mass to throat separation ratio. If $\mu_0 \simeq 1.8$, then black holes have the same event horizon. Similar solutions can be constructed for multiple black holes which has similar structure of space-time as shown in Figure 5.2 but connected by multiple stationary throats. For Misner initial data, the relation for ADM mass is given by

$$M = 4 \sum_{n=1}^{n=\infty} \frac{1}{\sinh(\mu_0 n)} \tag{5.5.8}$$

5.6 Results and Discussion

The platform chosen for our simulation of binary black hole space-time is Cactus. Cactus is an open source framework developed for scientists and engineers which have the capacity to run on a wide range of architectures and operating systems. Cactus gives the power of parallel computing for challenging and exhaustive simulations with its modular structure of thorns. There are two components to Cactus the basic functional and interface is provided by flesh the core module, while several other modules named as thorns have their respective specialized functionalities [13].

The emphasis of our simulation was on evolutions using the Schwarzschild and Misner initial data sets. There were 100x100x100 grid points to cover the whole space-time. Each run was done with aid of both fixed mesh refinement (FMR) and adaptive mesh refinement (AMR) techniques. AMR capabilities were provided by Carpet which is designed to work seamlessly with Cactus environment. The initial data were evolved by both BSSN and ADM formulation to test the reliability and crash times for code. ADM evolution is implemented in standard CactusEinstein thorns while BSSN functionality is provided by AEIThorns or CACTIE code. The Weyl scalars were extracted by PsiKadelia thorn measure the outgoing gravitational waves by the single static and dynamic binary black holes.

5.6.1 Schwarzschild Initial Data Evolution

The Schwarzschild black hole is a static solution to Einstein's equations. It represents the exterior of uncharged non-rotating black hole. However, this test run works as a benchmark for the code reliability and determining crash time. We have evolved initial data with ADM formalism based on FMR to about 17M with grid resolution of 0.2 and isotropic lapse. Such evolution has no interesting dynamics in it but Weyl scalars extracted showed some form of instability which eventually crashed at about 17M. Similar evolution was performed with the 1+log slicing and black hole mass of 1M. On contrary to isotropic lapse, such evolution showed some form of gauge waves. Perhaps, the reason for appearance of waves is that the resulting Schwarzschild isotropic metric was not in isotropic coordinates as it doesn't satisfy 1+log slicing condition. But still the precise description of waves is not known.

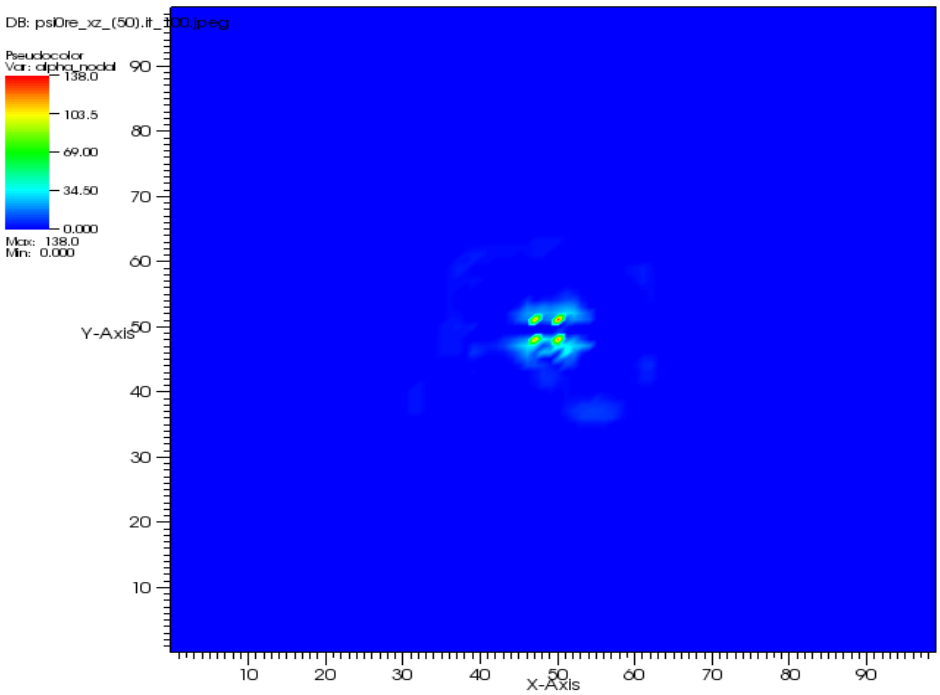

(a)

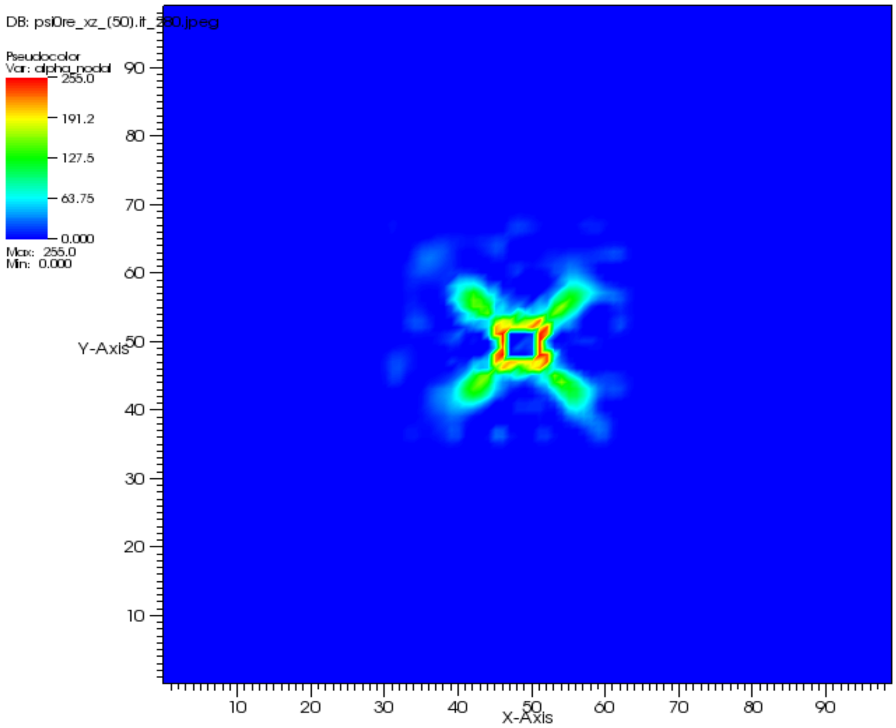

(b)

Figure 5.3. Evolution of Schwarzschild initial data with grid resolution 0.2 and isotropic lapse where boundary was placed at 10M. (a) Real part of Weyl scalar ψ_4 (outgoing transverse wave) at 5M in x-z. (b) Real part of Weyl scalar ψ_4 (outgoing transverse wave) at 14M in x-z plane. Beyond that instability overcomes.

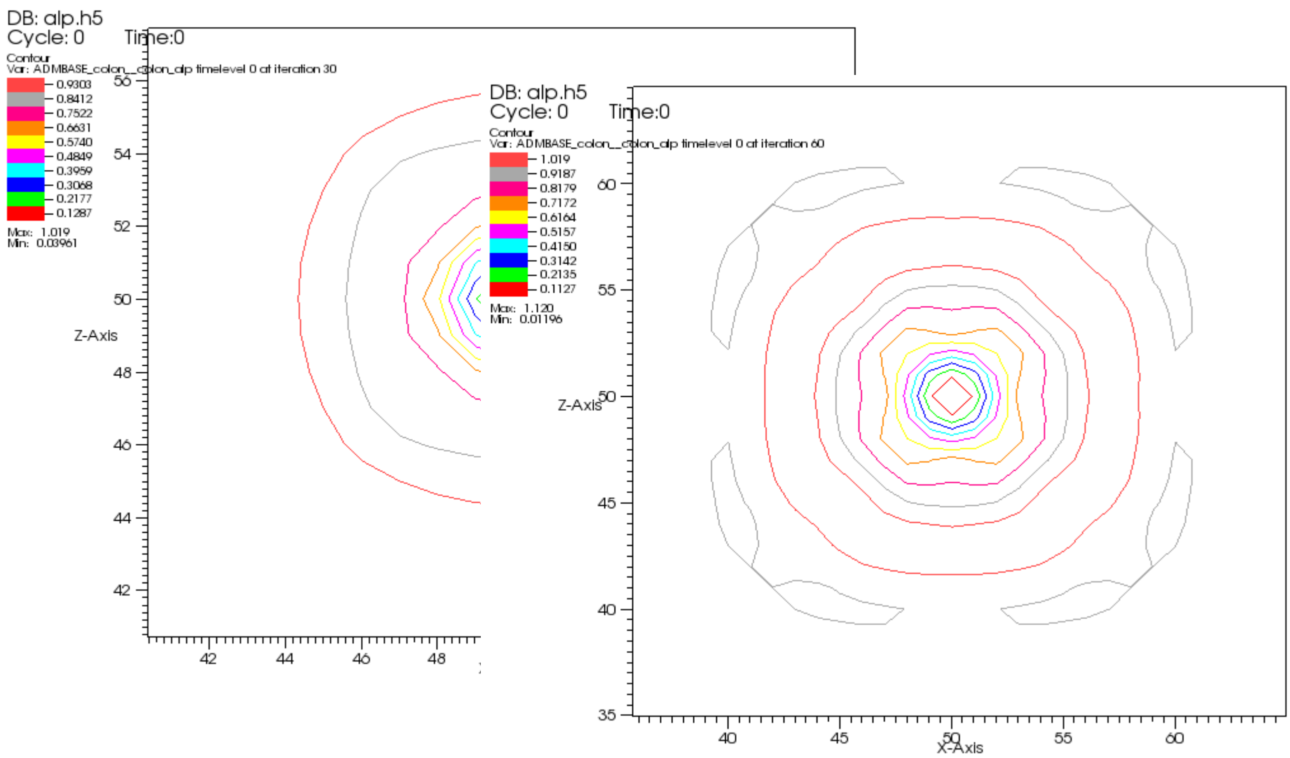

(c)

Figure 5.4. Evolution of Schwarzschild initial data with grid resolution 2 and 1+log lapse where boundary was at 100M. (a) The lapse contours at time 15M. (b) The lapse contours at time 30M. (c) Real part of Weyl scalar ψ_4 (outgoing transverse wave) at 30M in x-z.

5.6.2 Misner Initial Data Evolution

This initial data is of most interest in our case. The data was evolved with both FMR and AMR grids. Similarly, both ADM and BSSN evolution sequences were executed with 1+log gauge conditions and $\mu_0 = 2.2$. However, with BSSN the initial data was a lot more stable. An obvious reflection appears at the boundary (at 10M quite near) when no boundary condition was set during BSSN evolution with grid resolution 0.2. The data was also evolved with boundary at 100M and grid resolution 2. During evolution, outgoing gravitational waves were extracted by Weyl scalars.

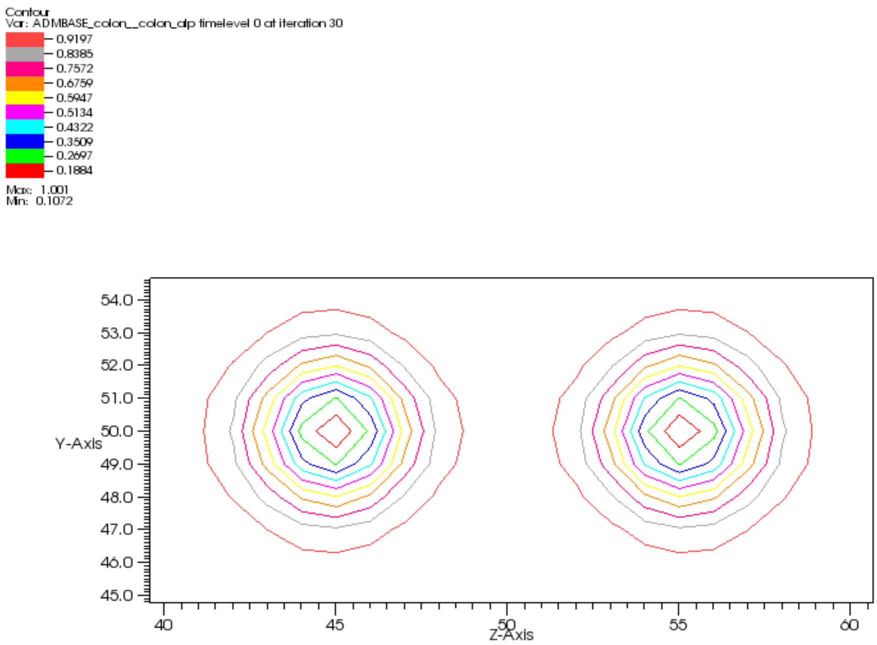

(a)

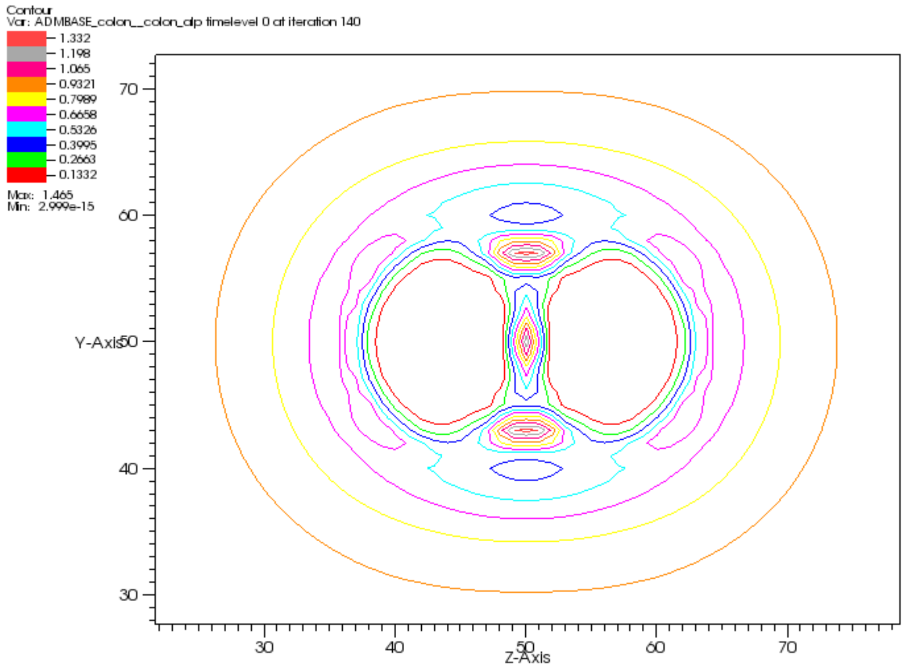
Contour
Var: ADMBASE_colon__colon_alp timelevel 0 at iteration 140
1.332
1.198
1.065
0.9321
0.7989
0.6658
0.5326
0.3995
0.2663
0.1332
Max: 1.465
Min: 2.999e-15
Y-Axis
Z-Axis

(b)

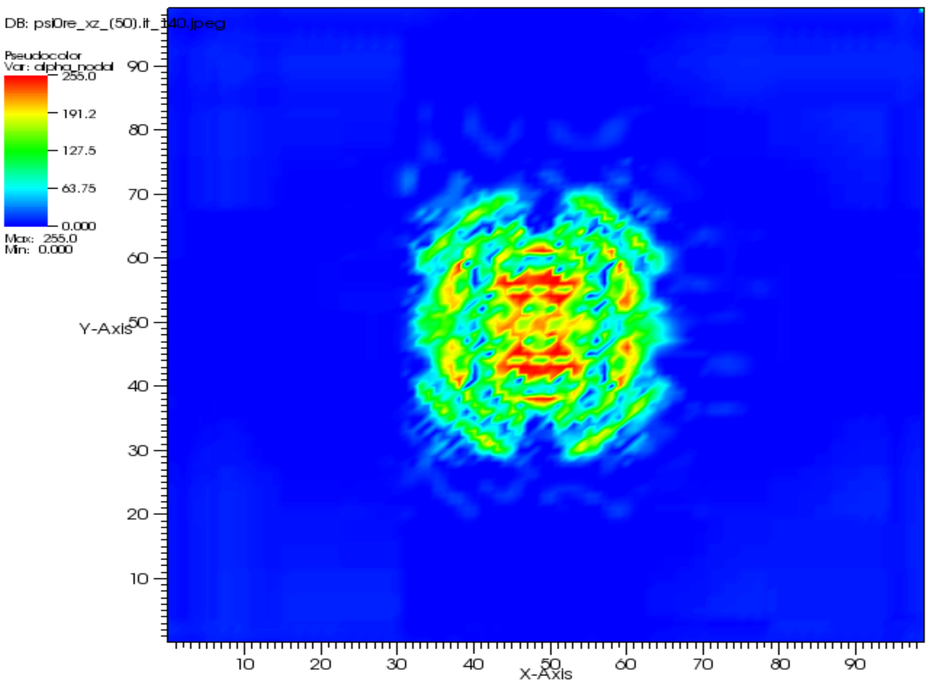
DB: psi0re_xz_(50).it_140.jpeg
Pseudocolor
Var: alpha_nodal
255.0
191.2
127.5
63.75
0.000
Max: 255.0
Min: 0.000
Y-Axis
X-Axis

(c)

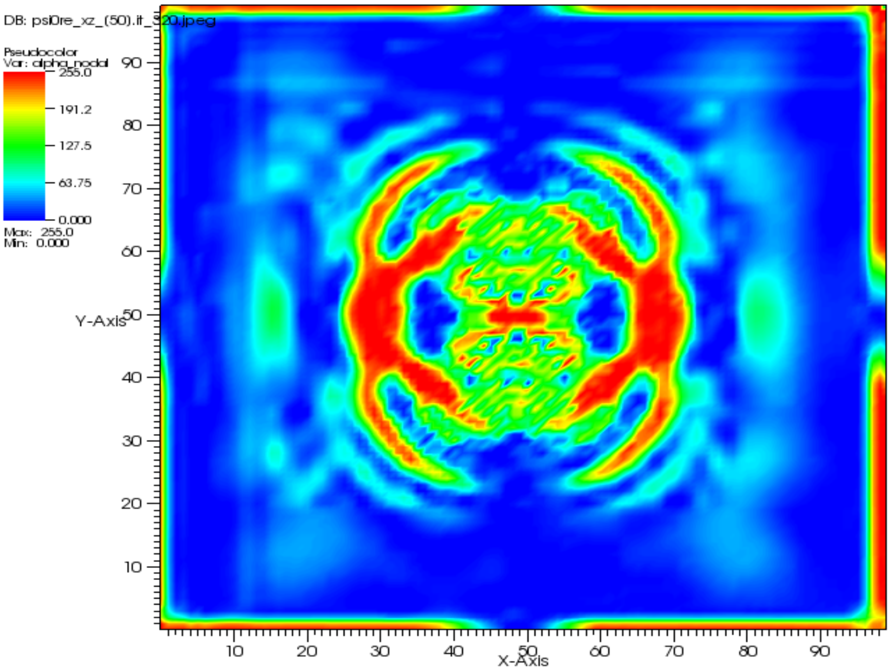
DB: psi0re_xz_(50).it_320.jpeg
Pseudocolor
Var: alpha_nodal
255.0
191.2
127.5
63.75
0.000
Max: 255.0
Min: 0.000
Y-Axis
X-Axis

(d)

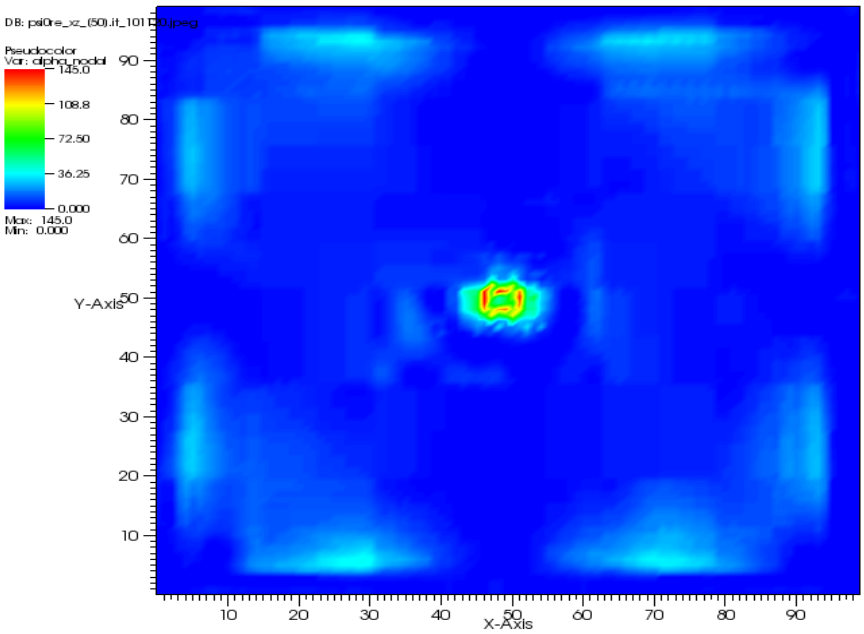
Pseudocolor
Var: alpha_nodal
145.0
108.8
72.50
36.25
0.000
Max: 145.0
Min: 0.000
Y-Axis
X-Axis

(e)

Figure 5.5. Evolution of Misner initial data with grid resolution of 0.2 where boundary is placed at 10M. (a) Lapse contour map at 1.5M with ADM evolution method using FMR. Lapse was initially set to unity. (b) Lapse at 7M for Misner initial data with ADM evolution method using FMR technique. (c) Real part of Weyl scalar ψ_4 (outgoing transverse wave) at 7M in x-z plane using FMR, The reflection is not apparent at boundaries with ADM evolution. (d) Real part of Weyl scalar ψ_4 (outgoing transverse wave) at 16M in x-z plane using FMR, The wave reflection at the boundary is at its peak with BSSN formulation. The apparent reflection is because no boundary condition was set throughout evolution and boundary has been place quite close. (e) Real part of Weyl scalar ψ_4 (outgoing transverse wave) at 20M in x-z plane, The wave reflection has been reduced due to radiative boundary condition with BSSN evolution and AMR.

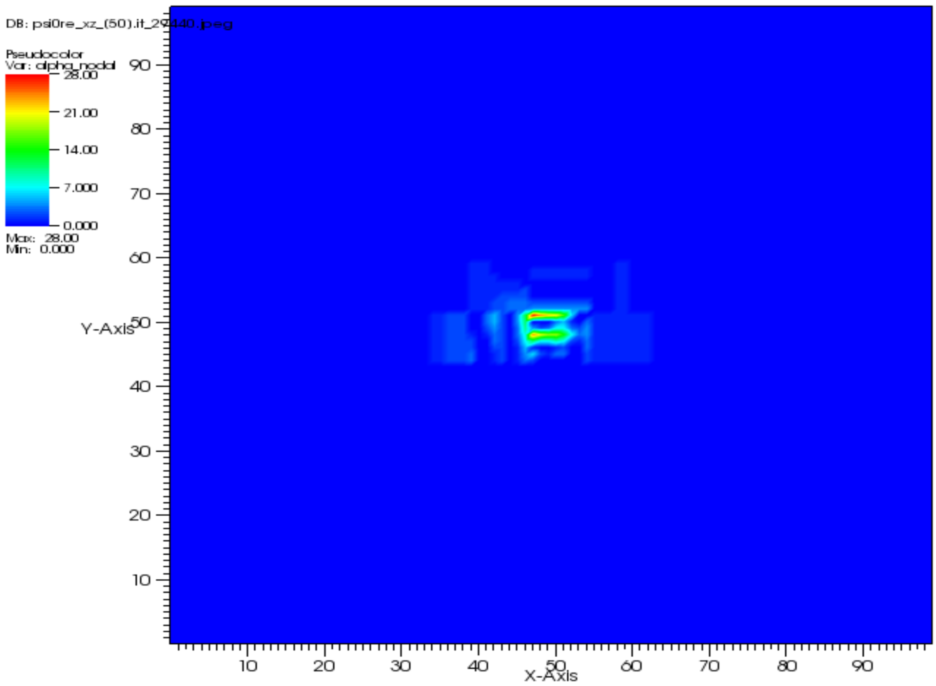

(a)

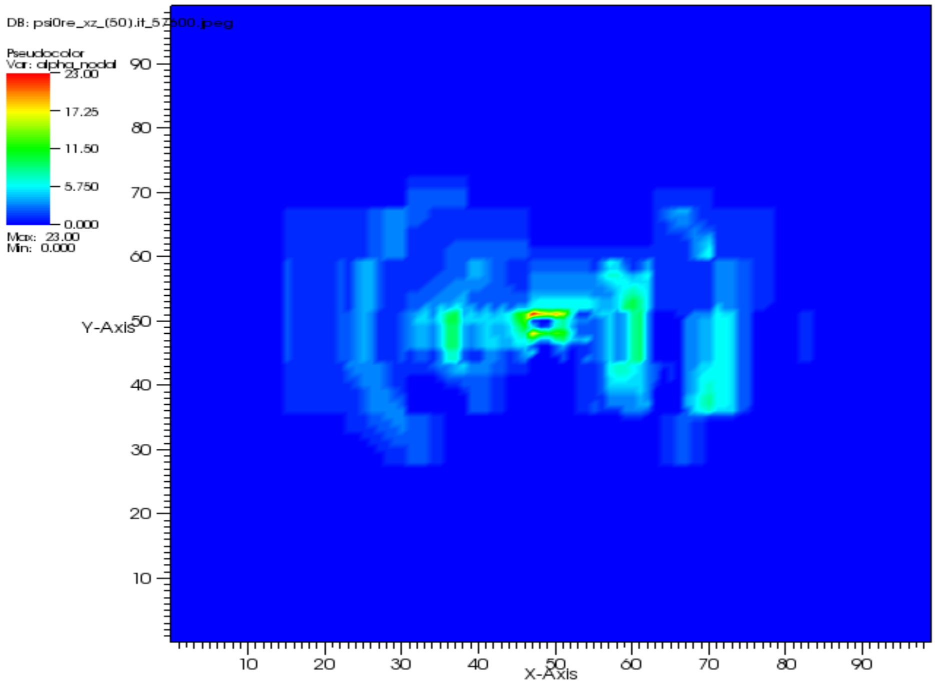
DB: psi0re_xz_(50).it_57600.jpeg
Pseudocolor
Var: alpha_nodal
23.00
17.25
11.50
5.750
0.000
Max: 23.00
Min: 0.000
Y-Axis
X-Axis
(b)

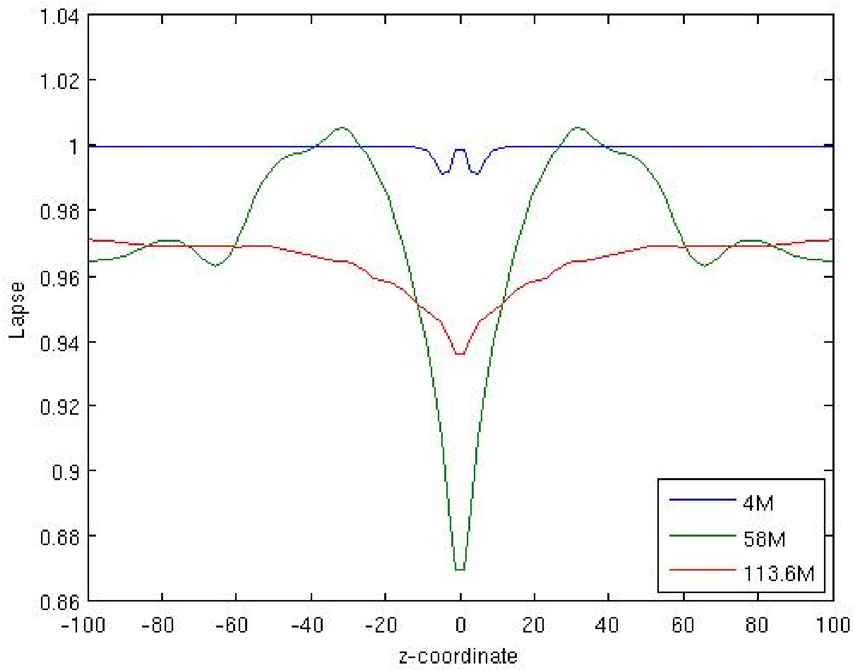
Lapse
z-coordinate
4M
58M
113.6M
(c)

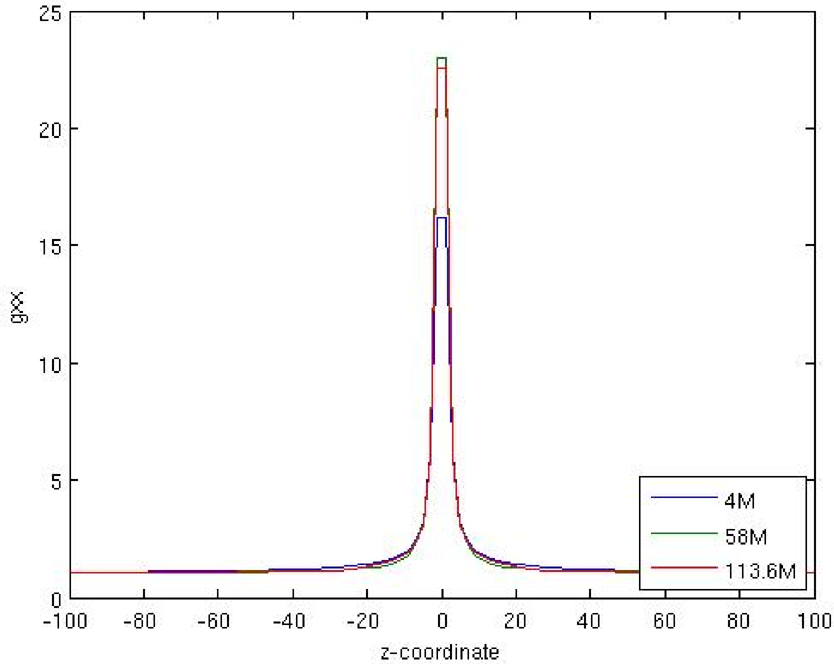

(d)

Figure 5.6. Evolution of Misner initial data with grid resolution of 2, where boundary is placed at 100M. (a) Real part of Weyl scalar ψ_4 (outgoing transverse wave) at 58M in x-z plane. (b) Real part of ψ_4 at 113.6M. (c)Evolution of lapse. (d) Evolution of gxx.

6 Conclusion and Future Work

The overall objective of this thesis was to carry out a study on gravitational waves, lay the theoretical foundation and test the findings by utilizing proper numerical tools available up to date. Due to the wide spectrum of this enriched area of study, it was impossible to even explore each and every subject in much detail. However, much have been done on extraction of gravitational waves during the inspiral and merger phase of the binaries. The pertinent concepts are touched in much detail for the foundation of future work. The extraction of waves by post-Newtonian formalism and simulating binary black hole space-time along with the extraction of Weyl scalars were explored with emphasis on computation.

The results obtained by aid of Cactus ware satisfactory. However, the emphasis of future work must rely on latest numerical relativity scenarios. Evolution of puncture method, thin sandwich data and extraction of various modes of Zerilli waves (Zerilli wave equation describe perturbations of non-rotating black hole) by simulating binaries to much longer times should be considered in future developments. Much more realistic grid sizes can be chosen which eventually requires more memory and time resources on the cluster. Various topics in this mature area are not even touched due to their complexity and shortage of time. The excision of black hole which is one of primary techniques of singularity avoidance is not mentioned in this thesis. Secondly, determination of black hole apparent horizons is also not treated, as much of our work was focussed on extraction of gravitational waves. The field of numerical relativity can be further explored by considering perturbed black holes, massive black holes inspiral and neutron stars merger.

References

1. Miguel Alcubierre, “Introduction to 3 + 1 Numerical Relativity”, Oxford University Press, 2008.

2. Kip S. Thorne, “Three hundred years of Gravitation: Gravitational Radiation”, Cambridge University Press. 1987.

3. Robert M.Wald, “General Relativity”, Chicago University Press, 1984.

4. Alessandra Buonanno, Bala R. Iyer, Evan Ochsner, Yi Pan and B. S. Sathyaprakash, “Comparison of post-Newtonian templates for compact binary inspiral signals in gravitational-wave detectors”, Phys.Rev.D 80, 084043, (2009), arXiv:0907.0700v1

5. Kip S. Thorne, “Multipole Expansion of Gravitational Radiation”, Reviews of Modern Physics Vol. 52, No. 2, Part I, 1980.

6. Toshifumi Futamase and Yousuke Itoh, “The Post-Newtonian Approximation for Relativistic Compact Binaries”, Living Rev. Relativity, 10, (2007), 2.

7. Charles W. Misner, Kip S. Thorne and John A. Wheeler , “Gravitation”, New York: W.H. Freeman and Company, 1973.

8. Jeffrey Winicour, “Characteristic Evolution and Matching”, Living Rev. Relativity, 12, (2009), 3.

9. Gregory B. Cook,”Initial Data for Numerical Relativity”, Living Rev. Relativity, 3, (2000), 5.

10. Beverly K. Berger, “Numerical Approaches to space-time Singularities”, Living Rev. Relativity, 5, (2002), 1.

11. Jonathan Thornburg, “Event and Apparent Horizon Finders for 3+1 Numerical Relativity”, Living Rev. Relativity, 10, (2007), 3.

12. Bernard F. Schutz, ”Gravitational Waves on the back of an envelope”, Am. J. Phys. 52, 412 (1984).

13. www.cactuscode.org

14. www.carpetcode.org

15. Michael Koppitz, “Numerical Studies of Black Hole Initial Data”, PhD thesis, University of Potsdam, 2004.

16. Lars Nerger, “Investigations of 3D Binary Black Hole Systems”, PhD thesis, AEI, 2000.

17. Karen D. Camarda, “A Numerical Study of 3D Black Hole space-times”, PhD thesis, University of Illinois at Urbana-Champaign, 1998.

18. Bernd Bruegmann, “Adaptive mesh and geodesically sliced Schwarzschild space-time in 3+1 dimensions”, Phys.Rev.D54:7361-7372,1996, arXiv:gr-qc/9608050v1

19. Peter Anninos, Karen Camarda, Joan Masso, Edward Seidel, Wai-Mo Suen, and John Towns, “Three dimensional numerical relativity: The evolution of black holes”, Phys.Rev. D52 (1995) 2059, 1995.

20. Markus P. Rumpfkeil, “Elliptic Gauge Conditions in Numerical Relativity”, Phd Thesis, Max-Planck Institute for Gravitational Astrophysics, 2004.

21. Ulrich Sperhake, “Black hole binary evolutions with the LEAN code”, Journal of Physics: Conference Series 66 (2007) 012049.

22. Michele Maggiore, “Gravitational Waves”, Oxford University Press, 2008.

23. www.chirplab.org

24. Luc Blanchet, “Post-Newtonian theory and the two-body problem”, arXiv:0907.3596v1

25. B.S. Sathyaprakash and Bernard F. Schtuz, “Physics, Astrophysics and Cosmology with Gravitational Waves”, Living Rev. Relativity, 12, (2009), 2

26. John Baker, Manuela Campanelli and Carlos O. Lousto, “The Lazarus project: A pragmatic approach to binary black hole evolutions”, Physical Review D, Vol 65, 044001, 2002.

27. Scott A. Hughes, Szabolcs Marka, Peter L. Bender, Craig J. Hogan, “New physics and astronomy with the new gravitational-wave observatories”, eConf C010630 (2001) P402, 2001.

28. Roger D. Blandford and Kip S. Thorne, ”Applications of Classical Physics”, 2008.

7 Appendix

A.1 Compiling and Running Cactus Framework

There are two important ingredients to setup framework for numerical relativity simulations. Primarily you will need to download Cactus [13] and compile it for your architecture and depending on the compilers and additional softwares you require, this will take some effort. Then you will need to download Carpet [14], a adaptive mesh refinement functionality which works well with the Cactus framework. First you will need to download Cactus from the following repository. I have tested this with OSX 1.6.2 with x-code 3.2. For this you need to have CVS and git on you system. Just you need to issue following commands

```
cvs -d :pserver:cvs_anon@cvs.cactuscode.org:/cactus login
```

You will be asked for password which is anon. After this you need to download Cactus flesh by command

```
cvs -d :pserver:cvs_anon@cvs.cactuscode.org:/cactus checkout Cactus
```

Similarly, you can checkout the others arrangements. Before that you need to go to Cactus/arrangements directory. The following arrangements are recommended and can be downloaded by the following command.

```
cvs -d :pserver:cvs_anon@cvs.cactuscode.org:/cactus checkout CactusEinstein
CactusWave CactusPUGH CactusPUGHIO CactusIO CactusExternal CactusConnect
CactusBase CactusBench CactusTest
```

Second step is to download Carpet by the issuing following commands

```
cd Cactus
git clone -o carpet     git://carpetcode.dyndns.org/carpet.git
cd arrangements
ln -s ../carpet/Carpet* .
```

The last command is just to create a software link. If your system does not support such command just create your own soft link and past it there. Before we continue to compiling, you need to have a C++/C and F77/F90 compiler. The best way you can get for your mac system is by website http://hpc.sourceforge.net/. Please download GCC 4.4 and install it from the binaries. The next you need to have a visualization software which I recommend is VisIT. Go to website https://wci.llnl.gov/codes/visit/executables.html get the executable and copy the install script along with it. Place both in the same directory and issue the following command. Remember this command is for the mac systems as mentioned before. Otherwise you need to make changes accordingly in the command.

```
sudo ./visit-install 1.12.1 darwin-i386 /visit
```

The third external software you need to have before we continue to compilation procedure is HDF5. Which you can get from http://www.hdfgroup.org/downloads. Get the current release of this software don't worry about the hdf5 software with the file streaming capabilities. The third repository you need to have is AEIThorns which you can have by

```
cvs -d :pserver:cvs_anon@cvs.aei.mpg.de:/numrelcvs login
CVS password: anon
cvs -d :pserver:cvs_anon@cvs.aei.mpg.de:/numrelcvs checkout AEIThorns
```

Now for configuration of Cactus on you local OSX machine issue following commands on terminal.

```
Cd Cactus
make local-config HDF5=yes LDFLAGS=-lgfortran F90=gfortran F77=gfortran
CC=gcc CXX=g++
```

This configures cactus with the config file name “local”. Make sure that cactus found the HDF directory and last test on compilers goes well. Now to compile this configuration write

```
make local
```

This will usually generate errors cause of incompatible thorns in your thorn list. So go to `Cactus/configs/local` folder and edit Thornlist file (just copy the thorns given below to you file and save it). The following thorns are recommended which are needed to be compile for purpose.

```
AEIThorns/AEILocalInterp           # AEILocalInterp ( ) [ ] { }
AEIThorns/AEIUtil                  # AEIUtil ( ) [ ] { }
AEIThorns/BAM_Elliptic             # BAM_Elliptic
AEIThorns/BAM_VecLap               # BAM_VecLap
AEIThorns/BSSN_MoL                 # adm_bssn
AEIThorns/BoundaryExample
AEIThorns/CalcK                    # CalcK (ADMBase,StaticConformal) [ ]
AEIThorns/Constants                # Constants ( ) [ ] { }
AEIThorns/EHFinder                 # ehfinder
AEIThorns/Exact                    # exact
AEIThorns/FiniteDifferencing       # FiniteDifferencing ( ) [ ] { }
AEIThorns/Fortran                  # Fortran ( ) [ ] { }
AEIThorns/HyperWave                # HyperWave (grid) [ ] {MethodOfLines}
AEIThorns/HyperWave0               # HyperWave0 (grid) [ ] { }
AEIThorns/IDConstraintViolate      # idconstraintviolate (admbase,grid) [ ]
AEIThorns/IDFileADM                # IDFileADM (ADMBase,StaticConformal,IO)
AEIThorns/ManualTermination        # ManualTermination ( ) [ ] { }
AEIThorns/Nice                     # nice ( ) [ ] { }
AEIThorns/Noise                    # Noise (grid) [ ] { }
AEIThorns/Norms                    # Norms ( ) [ ] { }
AEIThorns/PointwiseDerivatives     # PointwiseDerivatives ( ) [ ] { }
AEIThorns/TensorTypes              # TensorTypes ( ) [ ] { }
AEIThorns/TestInterpLocal_Large    # testinterplocal ( ) [ ] { }
AEIThorns/TestInterpLocal_Small    # testinterplocal ( ) [ ] { }
AEIThorns/TestInterpPUGH_Small     # testinterppugh ( ) [ ] { }


CactusEinstein/ADM
CactusEinstein/Extract
CactusEinstein/AHFinder
CactusEinstein/PsiKadelia
CactusEinstein/TimeGeodesic
CactusEinstein/IDAnalyticBH
CactusEinstein/IDSimple            # IDSimple
CactusEinstein/EvolSimple          # simple_adm
CactusEinstein/ADMAnalysis         # ADMAnalysis
CactusEinstein/ADMBase             # ADMBase (grid) [ ] { }
CactusEinstein/ADMConstraints      # admconstraints
CactusEinstein/ADMCoupling         # ADMCoupling ( ) [ ] { }
CactusEinstein/ADMMacros           # ADMMacros ( ) [ ] { }
CactusEinstein/SpaceMask           # SpaceMask (grid) [ ] { }
CactusEinstein/StaticConformal     # StaticConformal (grid) [ ] {ADMBase}
CactusEinstein/CoordGauge          # CoordGauge ( ) [ ] {ADMBase}

CactusElliptic/EllBase             # ellbase ( ) [ ] { }
CactusElliptic/EllSOR              # ellsor (ellbase,boundary) [ ]

CactusIO/IOJpeg                    # IOJpeg (IO) [ ] {IO}
CactusExternal/jpeg6b              # jpeg6b ( ) [ ] { }
CactusExternal/HDF5                # HDF5 ( ) [ ] { }
CactusExternal/FlexIO              # FlexIO ( ) [ ] { }

CactusUtils/NaNChecker

CactusConnect/HTTPD
CactusConnect/HTTPDExtra
CactusConnect/Socket
```

```
CactusPUGH/PUGH                   # Driver ( ) [ ] {cactus}
CactusPUGH/PUGHInterp             # Interp ( ) [ ] { }
CactusPUGH/PUGHReduce             # Reduce ( ) [ ] { }
CactusPUGH/PUGHSlab               # Hyperslab ( ) [ ] { }

CactusPUGHIO/IOFlexIO             # IOFlexIO (IO) [ ] {IO}
CactusPUGHIO/IOHDF5               # IOHDF5 ( ) [ ] {IO}
CactusPUGHIO/IOHDF5Util           # IOHDF5Util (IO) [ ] {IO}
CactusPUGHIO/IsoSurfacer          # isosurfacer (Grid,IO) [ ] {IO}

CactusBase/Boundary               # boundary ( ) [ ] { }
CactusBase/CartGrid3D             # grid (coordbase) [ ] {driver}
CactusBase/CoordBase              # CoordBase ( ) [ ] { }
CactusBase/IOASCII                # IOASCII ( ) [ ] {IO}
CactusBase/IOBasic                # IOBasic (IO) [ ] {IO}
CactusBase/IOUtil                 # IO ( ) [ ] { }
CactusBase/InitBase               # InitBase ( ) [ ] { }
CactusBase/LocalInterp            # LocalInterp ( ) [ ] { }
CactusBase/LocalReduce            # LocalReduce ( ) [ ] { }
CactusBase/MoL                    # MethodOfLines ( ) [ ] { }
CactusBase/SymBase                # SymBase ( ) [ ] { }
CactusBase/Time                   # time ( ) [ ] {cactus}

CactusWave/WaveToyC
CactusWave/IDScalarWaveC
CactusWave/WaveBinarySource
```

Now to run the parameter file test.par which you have written by issue the following command after cd to Cactus directory. The parameter file needed to be in the Cactus main directory.

```
./exe/cactus_local test.par
```

The task of configuration of Cactus on ada-cluster is slight different. First we don't have the HDF5 capability secondly we need to have MPI loaded before configuration. So after login to ada-cluster load following softwares

```
module load gcc/4.3.2 openmpi/1.3/gcc/4.1
```

Now make configuration file like we did on local mac-machine by command

```
make local-config  F90=mpif90 F77=mpif77 CC=mpicc CXX=mpic++ LDFLAGS=-
lgfortran  CFLAGS=-fgnu89-inline  MPI=OpenMPI
OPENMPI_DIR=openmpi/1.3/gcc/4.1
```

Then just make this configuration which will again generate errors. So again edit the Thornlist file by the below thorns (just paste the given Thornlist below and save the file).

```
# arrangement/thorn               # implements (inherits) [friend]
{shares}

AEIThorns/AEILocalInterp          # AEILocalInterp ( ) [ ] { }
AEIThorns/AEIUtil                 # AEIUtil ( ) [ ] { }
AEIThorns/AHFinderDirect          # AHFinderDirect
AEIThorns/BAM_Elliptic            # BAM_Elliptic
AEIThorns/BAM_VecLap              # BAM_VecLap
AEIThorns/BSSN_MoL                # adm_bssn
AEIThorns/BoundaryExample
AEIThorns/CalcK                   # CalcK (ADMBase,StaticConformal) [ ]
AEIThorns/Constants               # Constants ( ) [ ] { }
```

```
AEIThorns/Dissipation               # Dissipation
AEIThorns/EHFinder                  # ehfinder
AEIThorns/Exact                     # exact
AEIThorns/FiniteDifferencing        # FiniteDifferencing ( ) [ ] { }
AEIThorns/Fortran                   # Fortran ( ) [ ] { }
AEIThorns/HyperWave                 # HyperWave (grid) [ ] {MethodOfLines}
AEIThorns/HyperWave0                # HyperWave0 (grid) [ ] { }
AEIThorns/IDConstraintViolate       # idconstraintviolate (admbase,grid) [ ]
AEIThorns/IDFileADM                 # IDFileADM (ADMBase,StaticConformal,IO)
AEIThorns/ManualTermination         # ManualTermination ( ) [ ] { }
AEIThorns/Nice                      # nice ( ) [ ] { }
AEIThorns/NoExcision                # NoExcision
AEIThorns/Noise                     # Noise (grid) [ ] { }
AEIThorns/Norms                     # Norms ( ) [ ] { }
AEIThorns/PointwiseDerivatives      # PointwiseDerivatives ( ) [ ] { }
AEIThorns/TensorTypes               # TensorTypes ( ) [ ] { }
AEIThorns/TestInterpLocal_Large     # testinterplocal ( ) [ ] { }
AEIThorns/TestInterpLocal_Small     # testinterplocal ( ) [ ] { }
AEIThorns/TestInterpPUGH_Small      # testinterppugh ( ) [ ] { }
AEIThorns/SphericalSurface

CactusUtils/NaNChecker

CactusEinstein/ADM
CactusEinstein/Extract
CactusEinstein/AHFinder
CactusEinstein/PsiKadelia
CactusEinstein/TimeGeodesic
CactusEinstein/IDAnalyticBH
CactusEinstein/IDSimple             # IDSimple
CactusEinstein/EvolSimple           # simple_adm
CactusEinstein/ADMAnalysis          # ADMAnalysis
CactusEinstein/ADMBase              # ADMBase (grid) [ ] { }
CactusEinstein/ADMConstraints       # admconstraints
CactusEinstein/ADMCoupling          # ADMCoupling ( ) [ ] { }
CactusEinstein/ADMMacros            # ADMMacros ( ) [ ] { }
CactusEinstein/SpaceMask            # SpaceMask (grid) [ ] { }
CactusEinstein/StaticConformal      # StaticConformal (grid) [ ] {ADMBase}
CactusEinstein/CoordGauge           # CoordGauge ( ) [ ] {ADMBase}

CactusElliptic/EllBase              # ellbase ( ) [ ] { }
CactusElliptic/EllSOR               # ellsor (ellbase,boundary) [ ]

CactusIO/IOJpeg                     # IOJpeg (IO) [ ] {IO}
CactusExternal/jpeg6b               # jpeg6b ( ) [ ] { }
CactusExternal/FlexIO               # FlexIO ( ) [ ] { }

CactusConnect/HTTPD
CactusConnect/HTTPDExtra
CactusConnect/Socket
CactusUtils/TimerReport

CactusPUGH/PUGH                     # Driver ( ) [ ] {cactus}
CactusPUGH/PUGHInterp               # Interp ( ) [ ] { }
CactusPUGH/PUGHReduce               # Reduce ( ) [ ] { }
CactusPUGH/PUGHSlab                 # Hyperslab ( ) [ ] { }

CactusPUGHIO/IOFlexIO               # IOFlexIO (IO) [ ] {IO}
CactusPUGHIO/IsoSurfacer            # isosurfacer (Grid,IO) [ ] {IO}

CactusBase/Boundary                 # boundary ( ) [ ] { }
CactusBase/CartGrid3D               # grid (coordbase) [ ] {driver}
CactusBase/CoordBase                # CoordBase ( ) [ ] { }
CactusBase/IOASCII                  # IOASCII ( ) [ ] {IO}
CactusBase/IOBasic                  # IOBasic (IO) [ ] {IO}
CactusBase/IOUtil                   # IO ( ) [ ] { }
CactusBase/InitBase                 # InitBase ( ) [ ] { }
```

```
CactusBase/LocalInterp            # LocalInterp ( ) [ ] { }
CactusBase/LocalReduce            # LocalReduce ( ) [ ] { }
CactusBase/MoL                    # MethodOfLines ( ) [ ] { }
CactusBase/SymBase                # SymBase ( ) [ ] { }
CactusBase/Time                   # time ( ) [ ] {cactus}

CactusWave/WaveToyC
CactusWave/IDScalarWaveC
CactusWave/WaveBinarySource

Carpet/Carpet                     # Driver ( ) [ ] {Cactus,IO}
Carpet/CarpetEvolutionMask        # CarpetEvolutionMask ( ) [ ] { }
Carpet/CarpetIOASCII              # IOASCII ( ) [ ] {IO}
Carpet/CarpetIOBasic              # IOBasic (IO) [ ] {IO}
Carpet/CarpetIOScalar             # IOScalar ( ) [ ] {IO}
Carpet/CarpetInterp               # interp ( ) [ ] {Cactus}
Carpet/CarpetLib                  # CarpetLib ( ) [ ] {IO}
Carpet/CarpetReduce               # reduce ( ) [ ] { }
Carpet/CarpetRegrid               # CarpetRegrid ( ) [ ] { }
Carpet/CarpetRegrid2              # CarpetRegrid2 ( ) [ ] { }
Carpet/CarpetSlab                 # Hyperslab ( ) [ ] { }
Carpet/CarpetTest                 # CarpetTest ( ) [ ] { }
Carpet/CarpetTracker              # CarpetTracker
(SphericalSurface,CarpetRegrid2) [ ] {SphericalSurface,CarpetRegrid2}
```

So, again you can run parameters file on ada-cluster by the very similar commands mentioned before. The script file used for executing jobs on ada-cluster is below

```
#PBS -M fahadn@student.chalmers.se
#PBS -m a
#PBS -q ada
#PBS -r n
#PBS -l walltime=01:00:00
# Request 1 processor (node)
#PBS -l nodes=12:ppn=4
#PBS -N Cactus

cd $PBS_O_WORKDIR

module load gcc/4.3.2 openmpi/1.3/gcc/4.1
cd Cactus
./exe/cactus_local test.par
```

Before I will list the parameter files for the various simulations we have done I would like to mentioned some handy commands which will be useful for simulation task. Remember to install VisIT in `/usr/local/` directory so that you can execute it by the ./visit command after cd to `/usr/local/visit/bin` directory. Secondly, the way to remote login on Chalmers studat server is by ssh command.

```
ssh -Y fahadn@remote2.studat.chalmers.se
```

After you gain access to studat you can now login to ada-cluster again by very similar command.

```
ssh  fahadn@ada.c3se.chalmers.se
```

The way to copy files from ada-cluster to you computer or vice versa is by first copy it to your directory at studat then copy it from there by the following series of commands

```
scp -r fahadn@ada.c3se.chalmers.se:Cactus/try try
```

```
scp -r fahadn@remote2.studat.chalmers.se:try try
```

Make sure you are login to studat but not to ada-cluster. This will copy Cactus/try directory to try folder at you studat account then to you local computer.

A.2 Cactus Parameters Files

```
# Misner Black Hole evolution with BSSN formulation and Carpet

ActiveThorns = "CoordBase SymBase time carpet carpetlib TimerReport
carpetregrid carpetreduce carpetslab boundary cartgrid3d bssn_mol
mol nanchecker idanalyticbh carpetioascii LocalInterp LocalReduce
ioutil iobasic admcoupling admbase admmacros coordgauge spacemask
staticconformal carpetevolutionmask SphericalSurface PsiKadelia
IOJpeg"

cactus::terminate = "time"
cactus::cctk_initial_time = 0
cactus::cctk_final_time = 100
Time::dtfac = 0.25

IO::out_dir = "try/"
IOJpeg::out_every               = 10
IOJpeg::out_vars                = "PsiKadelia::WeylComponents"
```

```
IOBasic::outInfo_every = 1

driver::global_nsize=100

grid::type = "byrange"
grid::xyzmax=100
grid::xyzmin=-100

grid::domain             = "full"
grid::avoid_origin      = "no"

Carpet::ghost_size = 3
Carpet::max_refinement_levels = 9
Carpet::buffer_width = 9

Carpet::prolongation_order_space = 5
Carpet::prolongation_order_time = 2

###################################################################

MoL::ODE_Method = "RK4"
MoL::MoL_Intermediate_Steps = 4
MoL::MoL_Num_Scratch_Levels = 1

ADMBase::metric_type = "physical"
ADMBase::initial_data = "misner_bh"
ADMBase::initial_lapse = "one"
ADMBase::lapse_evolution_method = "1+log"
ADMBase::evolution_method = "ADM_BSSN"

ADMMacros::spatial_order = 4
ADMBase::initial_shift = "zero"

ADM_BSSN::timelevels = 3
ADM_BSSN::stencil_size = 3
ADM_BSSN::advection = "upwind4"
ADM_BSSN::bound = "newrad"
Boundary::radpower     = 3

ADM_BSSN::lapsesource = "straight"
ADM_BSSN::harmonic_f = 2.0
ADM_BSSN::force_lapse_positive = yes
ADM_BSSN::lapse_advection_coeff = 1.0

ADMBase::shift_evolution_method = "gamma0"
ADM_BSSN::ShiftGammaCoeff = 0.75
ADM_BSSN::BetaDriver = 1.0
ADM_BSSN::gamma_driver_advection_coeff = 1.0
ADM_BSSN::ApplyShiftBoundary = yes
```

```
# Misner Black Holes with BSSN formulation and Fixed Mesh Refinement

ActiveThorns = "boundary cartgrid3d time ioBasic admBase staticconformal
IDAnalyticBH ADMConstraints AHFinder Extract ADMCoupling ADM ADMMacros
CoordBase Coordgauge IOUtil spacemask PUGH ADMBase PUGHreduce SymBase
iojpeg jpeg6b InitBase LocalInterp LocalReduce admanalysis ioascii PUGHSlab
PUGHInterp PsiKadelia MoL BSSN_MoL IOHDF5 IOHDF5Util"

###################### Grid and Initial Setup Routines ##################

driver::global_nsize = 100
```

```
grid::type = "byrange"

# [-10M,10M]^3
grid::xyzmax = 10
grid::xyzmin = -10

# thus  20M/100 = 0.2M   dx=dy=dz=0.2M  as 0.2M resolves BH raduis
# typical grid size [-100M,100M]^3 for 3D Data

cactus::terminate = "time"
#cactus::cctk_initial_time = 0

# typical times for coalescence 10^2M-10^3M
cactus::cctk_final_time = 16.5


time::timestep_method = "courant_static"
time::dtfac = 0.25
IOBasic::outInfo_vars = "admbase::alp"
IOBasic::outInfo_every = 10

#IOASCII::out1D_vars = "admbase::alp admanalysis::grr PsiKadelia::psi0re
PsiKadelia::psi0im"
#IOASCII::out1D_every = 10
IO::out_dir = "try/"

#Outgoing gravitational waves psi0 INgoing psi4

IOHDF5::out_every = 10
IOHDF5::out_vars = "PsiKadelia::WeylComponents admbase::alp"

##########################################################################

admbase::evolution_method = "ADM_BSSN"
admbase::initial_lapse = "one"
ADMBase::initial_shift = "zero"
admbase::lapse_evolution_method = "1+log"
ADM_BSSN::bound = "none"
admbase::initial_data = "misner_bh"
idanalyticbh::mu = 2.2

ADM_BSSN::lapsesource = "straight"
ADM_BSSN::harmonic_f = 2.0
ADM_BSSN::force_lapse_positive = yes
ADM_BSSN::lapse_advection_coeff = 1.0
ADMBase::shift_evolution_method = "gamma0"
ADM_BSSN::ShiftGammaCoeff = 0.75
ADM_BSSN::BetaDriver = 1.0
ADM_BSSN::gamma_driver_advection_coeff = 1.0
ADM_BSSN::ApplyShiftBoundary = yes
```

```
# Schwarzschild Black Hole with FMR and ADM evolution

ActiveThorns = "boundary cartgrid3d time ioBasic admBase staticconformal
IDAnalyticBH ADMConstraints AHFinder Extract ADMCoupling ADM ADMMacros
CoordBase Coordgauge IOUtil spacemask PUGH ADMBase PUGHreduce SymBase
iojpeg jpeg6b InitBase LocalInterp LocalReduce admanalysis ioascii PUGHSlab
PUGHInterp PsiKadelia IOHDF5 IOHDF5Util"

##########################################################################

driver::global_nsize = 100
```

```
grid::type = "byrange"

# [-10M,10M]^3
grid::xyzmax = 10.0
grid::xyzmin = -10.0

# thus  20M/100 = 0.2M   dx=dy=dz=0.2M  as 0.2M resolves BH raduis
# typical grid size [-100M,100M]^3 for 3D Data

cactus::terminate = "time"
#cactus::cctk_initial_time = 0

# typical times for coalescence 10^2M-10^3M
cactus::cctk_final_time = 30
#cactus::cctk_itlast = 250


time::timestep_method = "courant_static"
time::dtfac = 0.25
IOBasic::outInfo_vars = "admbase::alp"
IOBasic::outInfo_every = 10
#IOASCII::out1D_vars = "admbase::alp admanalysis::grr PsiKadelia::psi0re
PsiKadelia::psi0im"
#IOASCII::out1D_every = 10
IO::out_dir = "try/"
IOJpeg::out_every              = 10
IOJpeg::out_vars               = "PsiKadelia::WeylComponents"
#IOJpeg::mode                   = "remove"
#IOJpeg::colormap               = "auto"
#IOJpeg::colormap_factor        = 16

#Outgoing gravitational waves psi0

IOHDF5::out_every = 10
IOHDF5::out_vars = "PsiKadelia::WeylComponents"

admbase::evolution_method = "ADM"
adm::method= "stagleap"
admbase::initial_lapse = "one"
admbase::lapse_evolution_method = "1+log"

admbase::metric_type = "static conformal"
admbase::initial_data = "schwarzschild"
idanalyticbh::mass = 1.0
```

 # Kerr Black Hole with FMR and ADM

```
ActiveThorns = "boundary cartgrid3d time ioBasic admBase staticconformal
IDAnalyticBH ADMConstraints AHFinder Extract ADMCoupling ADM ADMMacros
CoordBase Coordgauge IOUtil spacemask PUGH ADMBase PUGHreduce SymBase
iojpeg jpeg6b InitBase LocalInterp LocalReduce admanalysis ioascii PUGHSlab
PUGHInterp PsiKadelia IOHDF5 IOHDF5Util"


driver::global_nsize = 100
grid::type = "byrange"

# [-10M,10M]^3
grid::xyzmax = 10.0
grid::xyzmin = -10.0

# thus  20M/100 = 0.2M   dx=dy=dz=0.2M  as 0.2M resolves BH raduis
# typical grid size [-100M,100M]^3 for 3D Data
```

```
cactus::terminate = "time"
#cactus::cctk_initial_time = 0

# typical times for coalescence 10^2M-10^3M
cactus::cctk_final_time = 10
#cactus::cctk_itlast = 250


time::timestep_method = "courant_static"
time::dtfac = 0.25
IOBasic::outInfo_vars = "admbase::alp"
IOBasic::outInfo_every = 10
#IOASCII::out1D_vars = "admbase::alp admanalysis::grr PsiKadelia::psi0re
PsiKadelia::psi0im"
#IOASCII::out1D_every = 10
IO::out_dir = "try/"
IOJpeg::out_every              = 10
IOJpeg::out_vars               = "PsiKadelia::WeylComponents"
#IOJpeg::mode                   = "remove"
#IOJpeg::colormap               = "auto"
#IOJpeg::colormap_factor        = 16

#Outgoing gravitational waves psi0

IOHDF5::out_every = 10
IOHDF5::out_vars = "PsiKadelia::WeylComponents"

admbase::evolution_method = "ADM"
adm::method= "stagleap"
admbase::lapse_evolution_method = "1+log"

admbase::metric_type = "static conformal"
admbase::initial_data = "kerr"
admbase::initial_lapse = "kerr"
admbase::initial_shift = "kerr"

idanalyticbh::mass = 1.0
#idanalyticticbh::a_kerr = 0.3
```

A.3 Simulation of Binary Inspiral - MATLAB Code

```
% Calculates Cross and Plus Component of Amplitude of h(t)
%
% inc = inclination
% D = Distance in meters
% t = time vector
% m1, m2 = masses of binaries
% tc = time for coalescence

function [Ap,Ac,f]=Amp(t, m1, m2, tc, inc, D)

  T0 = 4.925E-06;     % (sec) for conversion of Mass to Geometrised units
(c=G=1)
  c = 3.0E+08;        % speed of light (m/sec)
  M = m1 + m2;        % total mass
  eta = m1*m2/(M^2); % symmetric mass ratio
  Mc = eta.^(3/5)*M; % Chirp Mass
  C = 1;              % C geometric factor
```

```
  f = freq(t, m1, m2, tc); %Calculating Instantaneous Frequency of GW

  Ac = -2*C*T0*c*Mc/D*(2*cos(inc))*(pi*Mc*T0*f).^(2/3);   %Cross Component
of h(t)
  Ap = (1 + cos(inc)^2) .* Ac./(2*cos(inc));                %Plus Component
of h(t)

return;
```

```
% Calculates Instantaneous Phase of GW
% p = instantaneous phase of GW
function p=phi(t, m1, m2, tc)

  T0 = 4.925E-06;     % sec, for Conversion to geometrized Units
  M = m1 + m2;        % total mass
  eta = m1*m2/(M^2); % symmetric mass ratio

  % Coefficients of expansion
  a0 = 1.0;
  a2 = 3715/8064 + 55/96*eta;
  a3 = -3*pi/4;
  a4 = 9275495/14450688 + 284875/258048*eta + 1855/2048*eta^2;


  theta = (eta*(tc - t)/(5*M*T0)).^(-1/8);
  p = -2/eta*theta.^(-5).*(a0 + a2*theta.^2 + a3*theta.^3 + a4*theta.^4);

return;
```

```
% Calculates Instantaneous frequency of the gravitational wave as a
function of t
% f= instantaneous freq

function f=freq(t, m1, m2, tc)

  T0 = 4.925E-06;     % seconds
  M = m1 + m2;        % total mass
  eta = m1*m2/(M^2); % symmetric mass ratio (unit-less)
  gamma = 0.577216;   % Euler constant
  theta = (eta*(tc - t)/(5*M*T0)).^(-1/8);


  % Coefficients of expansion
  a2 = 743/2688 + 11/32*eta;
  a3 = -3*pi/10;
  a4 = 1855099/14450688 + 56975/258048*eta + 371/2048*eta^2;
  a5 = (7729/21504 - 13/256*eta)*pi;
  a6= - 720817631400877/288412611379200 + 53/200*pi^2 + 107/280*gamma +
( 25302017977/4161798144 -       451/2048*pi^2)*eta - 30913/1835008*eta^2
+235925/1769472*eta^3 + 107/280*log(2.*theta);
  a7 = (-188516689/433520640 - 97765/258048*eta + 141769/1290240*eta^2)*pi;

  f = theta.^3/(8*pi*M*T0).*(1 + a2*theta.^2+ a3*theta.^3 + a4*theta.^4 +
a5*theta.^5 + a6.*theta.^6       + a7*theta.^7);

return;
```

```
% Calculate time as a function of velocity
% v = instantaneous velocity
```

```
function t=tv(v, m1, m2, tc)

  T0 = 4.925E-06;     % (seconds)
  M = m1 + m2;        % total mass
  eta = m1*m2/(M^2); % symmetric mass ratio (unit-less)

  % Coefficients of expansion up to 3.5 PN
  a0 = 1.0;
  a2 = 743/252 + 11/3*eta;
  a3 = -32*pi/5;
  a4 = 3058673/508032 + 5429/504*eta + 617/72*eta^2;
  a5 = (7729/252 - 13/3*eta)*pi;
  a6 = -10052469856691/23471078400 + 128/3*pi^2 + 6848/105*gamma +
(31477553127/3048192 -          451/12*pi^2)*eta -
15211/1728*eta^2+25565/1296*eta^3+3424/105.*log(16*v.^2);
  a7 = (-15419335/127008 - 75703/756*eta + 14809/378*eta^2)*pi;

  t = tc - 5*M*T0/(256*eta)*v.^(-8).*(a0 + a2*v.^2 + a3*v.^3 + a4*v.^4 +
a5*v.^5 + a6.*v.^6 + a7*v.^7);

return;
```

```
% Calculate velocity-squared as a function of time

function v2=v2t(t, m1, m2, tc)

T0 = 4.925E-06;     % (seconds)
M = m1 + m2;        % total mass
eta = m1*m2/(M^2); % symmetric mass ratio (unit-less)

% Determines v^2 from expression of t(v)
% by finding roots of the equation by considering it as polynomial in v^2
% instead of v -- see routine tv for expression

ct = (t - tc)*256*eta/(5*M*T0);
v2 = zeros(1, length(t));

c = zeros(1, 5);

c(5) = 1.0;
c(4) = 743/252 + 11/3*eta;

for k = 1:length(ct)
    c(1) = ct(k);
    r = roots(c);
    v2(k) = max(r);
end;

return;
```

```
% Calculates velocity v(t)

function v=vt(t, m1, m2, tc)

T0 = 4.925E-06;     % (seconds)
M = m1 + m2;        % total mass
eta = m1*m2/(M^2); % symmetric mass ratio (unit-less)


% v(t) is determined by the expression of t(v) by finding roots of the
% equation -- see routine 'tv' for expression
ct = (t - tc)*256*eta/(5*M*T0);
```

```
v = zeros(1, length(t));
c = zeros(1, 9);

c(9) = 1.0;
c(7) = 743/252 + 11/3*eta;
c(6) = -32*pi/5;
c(5) = 3058673/508032 + 5429/504*eta + 617/72*eta^2;
c(4) = (7729/252 - 13/3*eta)*pi;

for k = 1:length(ct)
    c(1) = ct(k);
    r = roots(c);     % finding roots of polynomial
    v(k) = max(r);    % just considering maximum root as solution
end;

return;
```

```
% Calculates the inspiral of binary
% f0 = reference frequency frequency at coalescence

function [h, p, f, Ap, Ac]=inspiral(t, m1, m2, tc, inc, f0)

  D = 1.0;  % Distance to binary from earth in meters

  p = phi(t, m1, m2, tc);
  [Ap,Ac,f] = Amp(t, m1, m2, tc, inc, D);
  h = Ap.*cos(p) + Ac.*sin(p);

  % Zero out everything where t >= tc
  % (after time of coalescence)
  h(t >= tc) = 0;
  p(t >= tc) = 0;
  f(t >= tc) = 0;
  Ap(t >= tc) = 0;
  Ac(t >= tc) = 0;

  % Zero out everything where inst. frequency is < f0
  % (larger then reference freq.)
  h(f < f0) = 0;
  p(f < f0) = 0;
  f(f < f0) = 0;
  Ap(f < f0) = 0;
  Ac(f < f0) = 0;

  % Normalize thats why D value doesn't matter
  h = h/norm(h);

return;
```

```
% Test for inspiral.m
% Neutron star binary inspiral (1.4-1.4 solar masses)
m1 = 1.4;            % mass of object 1 (solar mass units)
m2 = 1.4;            % mass of object 2 (solar mass units)
srate = 2048;        % sample rate (Hz)
tc = 32.0;           % time taken for coalescence (seconds)
inc = 0.0;             % angle of inclination
f0 = 40.0;           % reference frequency (Hz) when binary is impossible to
detect by LIGO
dt = 1/srate;        % sample size (seconds)
N = floor(srate*tc);   % Number of data points needed
t = [0:N-1].'*dt;      % Time parameter
```

```
[h, p, f] = inspiral(t, m1, m2, tc, inc, f0);
figure,

figure, plot(t, p);
axis tight
xlabel('Time (sec)');
ylabel('\phi(t)');
title('Binary inspiral waveform');

figure, plot(t, f);
axis tight
xlabel('Time (sec)');
ylabel('F(t)');

figure, plot(t, h);
axis tight
xlabel('Time (sec)');
ylabel('h(t)');

figure,
specgram(h, Nfft, srate, Nfft/2);
```

```
% Test Neutron star binary inspiral (1.4-1.4 solar masses)
m1 = 1.4;           % mass of object 1 (solar masses)
m2 = 1.4;           % mass of object 2 (solar masses)
tc = 32.0;          % time to coalescence (seconds)
srate = 2048;       % sample rate (Hz)
dt = 1/srate;
N = tc*srate;

t = (0:N-1)*dt;  % time vector
phase = phi(t, m1, m2, tc);
f = freq(t, m1, m2, tc);
v2 = v2t(t, m1, m2, tc);
h = v2.*cos(phase);      % amplitude is approximated by v^2 more accurately

figure,
plot(t, phase);
axis tight
xlabel('time (sec)');
ylabel('\phi(t)');

figure,
plot(t, f);
axis tight;
xlabel('time (sec)');
ylabel('F(t)');

figure,
plot(t, h);
axis tight;
xlabel('time (sec)');
ylabel('h(t)');

figure,
Nfft = 512;
specgram(h, Nfft, srate, Nfft/2);
```

```
% Calculates Inspiral with stationary phase approximation

function [h t]=inspiralsphase(m1, m2,srate,tc,f0)

T0 = 4.925E-06;              % conversion factor to geometrised units (sec)
M = m1 + m2;                 % total mass
```

```
eta = m1*m2/(M^2);            % symmetric mass ratio (unitless)
N = 2^nextpow2(tc*srate);     % number of samples
T = N/srate;                  % actual length of sequence (seconds)
Nyq = srate/2.0;              % Nyquist frequency (Hz)
dt = 1/srate;                 % time-step size (seconds)
df = srate/N;                 % frequency-step size (Hz)
t = 0:N-1*dt;

f = (1:N/2-1)*df;    % positive frequencies, up to but not including Nyq,
                     % used for calculating chirp as a function of frequency
                     % (zero excluded to prevent divide-by-zero later)

% Calculate Si(f) in frequency domain
si = 2*pi*tc.*f +tc+ ( (3/(128*eta))*(pi*T0*M)^(-5/3) )*f.^(-5/3) +
(3715/756+55/9*eta)*(3/(128*eta))*(pi*M*T0)^-1*f.^-1;
chirp = f.^(-7/6).*exp(-1i*si+pi/4);

c = [ 0 chirp ];    % DC component which is zero
f = [ 0 f ];

w = zeros(1, length(f));
w(f0 <= f) = 1.0;

c = w.*c;     % Boxcar multiplication
figure,plot(abs(c))

% inserting Spectrum at Nyquist frequencies of a real signal
H = [ c 0 conj(c(end:-1:2)) ];
figure,plot(abs(H))

% Inverse fourirer transform
h = real(ifft(H));

% kill everything below (T - tc)
h = h((T-tc) <= t);

% time vector of new h(t)
t = (0:length(h)-1)*dt;

%Removing artifatcs in Lower and high frequency
[b, a] = butter(4, 1.4*f0/Nyq, 'high');
h = filter(b, a, h);

 figure,
 [x,y,z] = butter(4,1.4*f0/Nyq,'high');
 [sos,g] = zp2sos(x,y,z);       % Convert to SOS form
 Hd = dfilt.df2tsos(sos,g);    % Create a dfilt object
 h = fvtool(Hd);               % Plot magnitude response
 set(h,'Analysis','freq')       % Display frequency response

[b, a] = butter(4, 0.98,'low');
h = filter(b, a, h);
 figure,
 [x,y,z] = butter(4,.98,'low');
 [sos,g] = zp2sos(x,y,z);       % Convert to SOS form
 Hd = dfilt.df2tsos(sos,g);    % Create a dfilt object
 h = fvtool(Hd);               % Plot magnitude response
 set(h,'Analysis','freq')       % Display frequency response

return;
```

```
% Test for inspiralsphase.m
% Neutron star binary inspiral (1.4-1.4 solar masses)
clc
m1 = 1.4;            % mass of object 1
```

```
m2 = 1.4;           % mass of object 2
srate = 2048;       % sample rate (Hz)
tc = 32.0;          % time from t = 0 to coalescence (seconds)
i = 0.0;            % angle of inclination
f0 = 40.0;          % reference frequency (Hz) when binary is impossible to
detect by LIGO
dt = 1/srate;       % sample size (seconds)
N = floor(srate*tc);    % Number of data points needed
t = (0:N-1).'*dt;       % Time parameter

[h t] = inspiralsphase(m1, m2, srate, tc,f0);
figure,
subplot(2, 1, 1);
plot(t,h);
axis tight
xlabel('Time (s)');
ylabel('h(t)');

figure,
Nfft = 512;
specgram(h, Nfft, srate, Nfft/2);
```